

# Free and forced morphodynamics of river bifurcations

M. Redolfi\*, G. Zolezzi\*, M. Tubino\*.

\* Department of Civil, Environmental and Mechanical Engineering, University of Trento, Italy

## Abstract

Water and sediment distribution by river bifurcations is often highly unbalanced. This may result from a variety of factors, like migration of bars, channel curvature, backwater effects, which promote an uneven partition of flow and sediment fluxes in the downstream branches, which we call “forcings”. Bifurcations also display an intrinsic instability mechanism that leads to unbalanced configurations, as it occurs in the idealized case of a geometrically symmetric bifurcation, which we call “free”, provided the width-to-depth ratio of the incoming flow is large enough. Most frequently, these free and forced mechanisms coexist, however their controlling roles on bifurcation dynamics has not been investigated so far. In this paper we address such question by proposing a unified free-forced modelling framework for bifurcation morphodynamics. Upstream channel curvature and different slopes of downstream branches (slope advantage) are specifically investigated as forcing effects typically occurring in bifurcations of alluvial channels. The modelling strategy is based on the widely used two-cell model of *Bolla Pittaluga et al.* (2003) here extended to account for the spatially non-uniform fluxes entering the bifurcation node. Results reveal that the relative role of free and forced mechanisms depends on the width to depth ratio falling above or below the resonant threshold that controls the stability of free bifurcations: when the main channel is relatively wide and shallow (super-resonant regime) the bifurcation invariably evolves towards unbalanced configurations, whatever the combination of curvature and slope advantage values, which instead control the bifurcation response under sub-resonant conditions. Detection of the resonant aspect ratio as a key threshold also releases the modelling approach from the need of parameter calibration that characterized previous approaches, and allows for interpreting under a unified framework the opposite behaviours shown by gravel bed and sand bed bifurcations for increasing Shields parameter values.

# 25 1 Introduction

26 Channel bifurcations control the downstream distribution of water and sediments in a variety of  
27 fluvial environments, such as deltas, alluvial fans, braided and anabranching rivers (*Slingerland*  
28 *and Smith, 2004; Kleinhans et al., 2013*). Understanding their dynamics is therefore important for  
29 managing water resources and the flooding risk, predicting the long-term morphological evolution  
30 of channel networks and evaluating the effectiveness over time of river restoration projects aimed  
31 at reactivating a multi-thread configuration (e.g., *Habersack and Piégay, 2007*). Bifurcation dy-  
32 namics also control instream processes in meander bends that mitigate the development of channel  
33 sinuosity through the occurrence of short cuts through point bars (*Grenfell et al., 2012; van Dijk*  
34 *et al., 2014*).

35 River bifurcations have been extensively studied through laboratory-scale physical models (*Fed-*  
36 *erici and Paola, 2003; Bertoldi and Tubino, 2007; Bertoldi et al., 2009; Le et al., 2018b*), and  
37 mathematical models based on 1D (*Wang et al., 1995; Bolla Pittaluga et al., 2003; Kleinhans*  
38 *et al., 2013; Salter et al., 2018*), 2D (*Edmonds and Slingerland, 2008; Siviglia et al., 2013; Le*  
39 *et al., 2018b,a*) and 3D approaches (*Kleinhans et al., 2008*). Along with field observations (e.g.,  
40 *Zolezzi et al., 2006; Kleinhans et al., 2012*), these studies highlight the almost invariable tendency  
41 of bifurcations to produce an uneven distribution of flow and sediment transport, which results in  
42 a strong asymmetry of the channel width and bed elevation of downstream anabranches.

43 This type of unbalanced configuration is often promoted by various “forcing” effects that drive  
44 the bifurcation towards an unbalanced state, sometimes leading to the complete closure of one  
45 of the anabranches. Forcing factors include both upstream and downstream effects. Upstream  
46 effects comprise mechanisms that feed the bifurcating node with a topographically-driven uneven  
47 distribution of flow and transport rate, like the curvature of the upstream channel (*Kleinhans*  
48 *et al., 2008; Hardy et al., 2011; Sloff and Mosselman, 2012*) and the occurrence of migrating  
49 bars (*Bertoldi et al., 2009; Bertoldi, 2012*) or steady bars (*Le et al., 2018b*). Downstream effects  
50 include mechanisms that provide, locally or through backwater effects, a slope advantage to one  
51 of the distributaries (*Edmonds, 2012; van Dijk et al., 2014; Zhang et al., 2017; Salter et al., 2018*).  
52 For purely illustrative purposes, Figure 1 shows real-world bifurcations with examples of these

53 concepts. Figures 1a and 1b provide examples of bifurcations where one of these forcing factors is  
54 likely dominant: the upstream channel curvature (Figure 1a) and the slope advantage for the right  
55 bifurcate (Figure 1b). In Figures 1c and 1d these two forcings likely have comparable relevance.  
56 They might cooperate in the case of Figure 1c, because the chute channel detaches from the outer  
57 bank of the upstream channel bend, thus receiving most of the water and sediment input from  
58 upstream, and is also shorter than the other (left) bifurcate, thus having a slope advantage. On  
59 the contrary, they likely compete in the case of Figure 1d, because the shorter chute channel occurs  
60 on the inner bank of the upstream channel bend.

61 Interestingly, the unbalanced configuration can also result from an inherent instability mecha-  
62 nism, even in the absence of external forcings, as shown theoretically by *Wang et al.* (1995) and  
63 *Bolla Pittaluga et al.* (2003), and later demonstrated through laboratory and numerical studies  
64 (*Bertoldi and Tubino, 2007; Edmonds and Slingerland, 2008; Siviglia et al., 2013; Salter et al.,*  
65 *2018*). More recently *Redolfi et al.* (2016) provided an interpretation of such “free” bifurcations  
66 instability within the framework of the theory of morphodynamic influence of *Zolezzi and Sem-*  
67 *inara* (2001), showing that the unbalanced configuration arises when the bifurcation is able to  
68 exert an upstream morphodynamic influence that allows for the formation of an upstream steady  
69 bar. Such upstream morphodynamic influence theoretically occurs when the width to depth ratio  
70 exceeds a threshold “resonant” value, as originally defined by *Blondeaux and Seminara* (1985) in  
71 the theory of regular meanders. For small (sub-resonant) values of the width to depth ratio a  
72 symmetric free bifurcation keeps stable and equally distributes water and sediment fluxes in the  
73 downstream branches, while in the super-resonant regime such balanced configuration is no longer  
74 stable and the bifurcation invariably evolves towards an unbalanced configuration.

75 The above scenario suggests that in sub-resonant conditions the tendency towards unbalanced  
76 states observed in real rivers is mainly driven by external forcing factors, while in super-resonant  
77 conditions both free and forced mechanisms are likely interacting, though their respective roles  
78 have not been investigated so far. The question therefore arises to which extent the autogenic, free-  
79 instability mechanism or instead the external forcings affect the behaviour of natural bifurcations,  
80 and under which conditions those effects cooperate or compete to produce what is observed in

81 such complex settings.

82 We aim at answering this question by taking the viewpoint of river bifurcations as dynamical  
83 systems for which a distinct role of the free and forced responses can be identified. This method-  
84 ological distinction is based on the recognition that free and forced mechanisms display substantial  
85 differences in their evolutionary temporal and spatial scales. Similar approaches have proven to  
86 provide thorough insight in the study of other morphodynamic processes, like the dynamics of  
87 river bars in curved or meandering channels (*Seminara and Tubino, 1989*), where migrating free  
88 bars develop on a much faster scale than that required to shape the meander planform (*Tubino  
89 and Seminara, 1990*).

90 In this paper we cast within a unified theoretical framework previous results on free and  
91 forced bifurcations and consider two main forcing factors: the upstream effect exerted by an  
92 incoming curved channel and the downstream effect of slope advantage of one of the distributaries,  
93 which can derive from the different length of the distributaries, from differential downstream  
94 degradation/deposition (*Salter et al., 2018*), or from backwater effects (e.g. *Edmonds, 2012*).

95 The analysis is based on the two-cell model originally proposed by *Bolla Pittaluga et al. (2003)*,  
96 as extended by *Kleinhans et al. (2008)* to account for the curvature-driven secondary flow, and on  
97 the theoretical results of *Redolfi et al. (2016)*. The analytical model prescribes physically-based,  
98 simplified nodal point relationships that enables us to explore the basic mechanisms that drive the  
99 water and sediment distribution at the node. As highlighted by *Wang et al. (1995)*, the behaviour  
100 of the bifurcation depends on how the sediment is distributed with respect to the downstream  
101 transport capacity; sediment distribution is in turn determined by the transverse flow-exchange  
102 and gravitational effects on bed load transport just upstream the bifurcation node, as explained  
103 by *Bolla Pittaluga et al. (2003)*.

## 104 **2 Methods**

105 Our model stems from the *Bolla Pittaluga et al. (2003)* two-cell approach, and is formulated to  
106 incorporate both free and forced bifurcation responses, and their interaction. It allows predicting  
107 how water and sediment fluxes delivered from the upstream main channel are drained by the

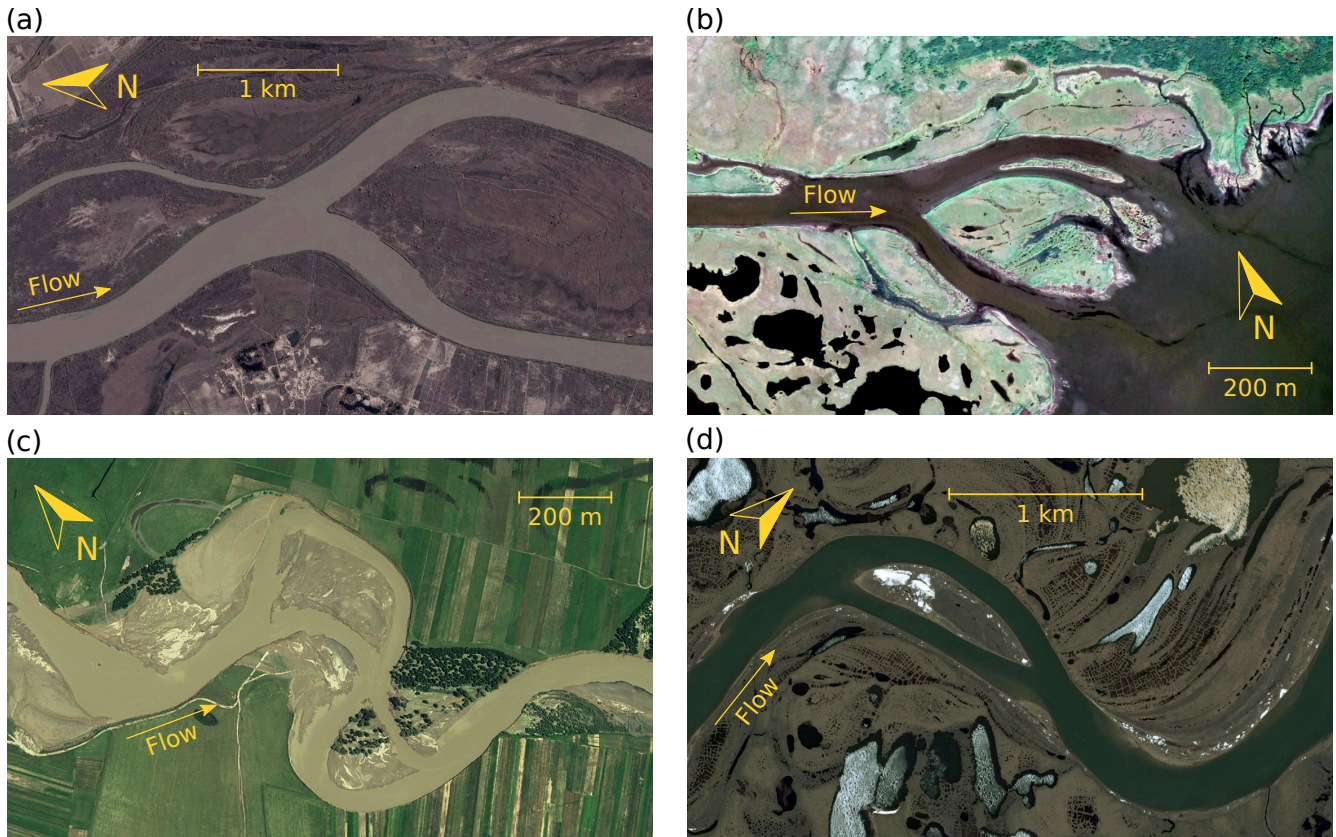


Figure 1: Satellite images showing illustrative examples of river bifurcations: (a) Tigris River near Baghdad (Iraq),  $34^{\circ}16' N$ ,  $43^{\circ}50' E$ , with a curved upstream channel and downstream bifurcates having a nearly symmetrical channel geometry; (b) estuary in the Kamchatka Peninsula (Russia),  $60^{\circ}02' N$ ,  $163^{\circ}40' E$ , where the left bifurcate likely covers a longer distance for the same elevation gap from the bifurcation node to the sea, suggesting a possible slope advantage for the left bifurcate; (c) bends with chute cutoffs in the meandering Siret River (Romania),  $47^{\circ}39' N$ ,  $26^{\circ}30' E$ , with the cutoff channel initiating on the outer bank of an upstream channel bend and being shorter than the left bifurcate; (d) meandering River in the Ust-Chaun area (Russia),  $68^{\circ}42' N$ ,  $170^{\circ}35' E$ , with the cutoff channel initiating on the inner bank of a bend and being shorter than the left bifurcate; from *Google Earth, Digital Globe (2018)*.

108 downstream anabranches, under different combination of external forcings.

109 The bifurcation geometry is sketched in Figure 2a, having an upstream, curved main channel  
 110 of width  $W_a$ , slope  $S_a$  and radius of curvature  $R$ , which bifurcates in two downstream channels  
 111 having width  $W_b$  and  $W_c$  and slope  $S_b$  and  $S_c$ , respectively. In the model, flow and sediment  
 112 balances applied to two cells of length  $\alpha W_a$ , which also accounts for transverse exchanges, rules  
 113 the distribution of water ( $Q$ ) and sediment ( $Q_s$ ) fluxes between the bifurcates, as represented in  
 114 Figures 2b and 2c.

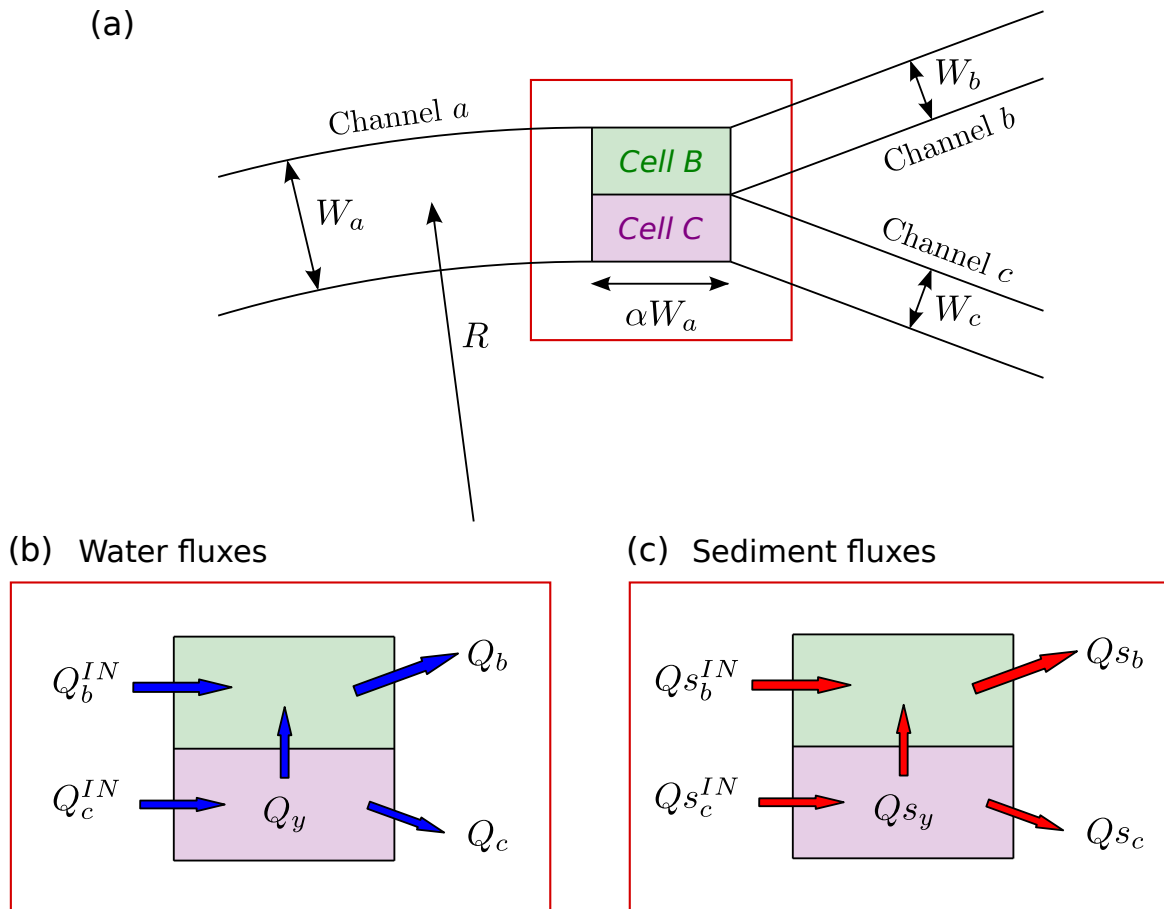


Figure 2: Bifurcation geometry and notation used in the mathematical model formulation: (a) planform view, showing the curved main channel, the two distributaries and the two cells; (b) and (c) water and sediment fluxes through the cells.

115 The model considers the effect of secondary flows associated with streamline curvature within  
 116 the node cells (*Kleinhans et al.*, 2008), and includes an extension of such previous model to account  
 117 for the non-uniform distribution for the entering water and sediment fluxes.

## 118 2.1 The free bifurcation

119 The core of the method is a model for a free bifurcation with perfectly symmetrical geometry and  
 120 boundary conditions (i.e. with no curvature nor slope advantage) that follows the classic approach  
 121 of *Bolla Pittaluga et al.* (2003). The flow and bed topography in the three channels result from  
 122 a 1D mobile bed model, which can be solved once the following five matching conditions at the  
 123 bifurcation node are specified: conservation of sediment and water fluxes (two conditions), energy  
 124 conservation (i.e. water surface elevation) along each cell (two conditions), and a physically-based  
 125 relation that prescribes how sediment fluxes are partitioned at the bifurcation node. This type  
 126 of nodal point relation is the key to incorporate bifurcation morphodynamics within a simple 1D  
 127 scheme, and accounts for the exchange of sediment between the two cells through the following  
 128 relationship:

$$\underbrace{\frac{Qs_y/(\alpha W_a)}{Qs_a/W_a}}_{\text{sediment flux direction}} = \underbrace{\frac{Q_y/(\alpha W_a D_{abc})}{Q_a/(W_a D_a)}}_{\text{velocity direction}} - \underbrace{\frac{2r}{\sqrt{\theta_a}} \frac{\eta_b - \eta_c}{W_b + W_c}}_{\text{gravitational effect}}, \quad (1)$$

129 where the direction of the sediment flux is determined by the direction of velocity and by the  
 130 gravitational effect induced by the transverse gradient of the bed elevation. The last term of  
 131 Equation (1) is estimated according to the *Ikeda* (1982) formulation, where  $r$  is a dimensionless  
 132 coefficient (e.g., *Baar et al.*, 2018),  $\theta_a$  is the Shields stress in the main Channel  $a$ ,  $\eta_b$  and  $\eta_c$  indicate  
 133 the bottom elevation at the inlet of the distributary Channels  $b$  and  $c$ , respectively. The mean  
 134 depth within the cell, defined as  $D_{abc} = (2D_a + D_b + D_c)/4$ , can be simplified to  $D_{abc} = D_a$  as  
 135 proposed by *Salter et al.* (2018).

136 The flow in the three anabranches is modelled using a classic 1D shallow water and Exner  
 137 model, whose steady solution is simply an uniform flow. The water flow in each channel  $i = \{a, b, c\}$   
 138 is given by:

$$Q_i = W_i c_i \sqrt{g S_i} D_i^{3/2}, \quad (2)$$

139 where  $g$  is the gravitational acceleration,  $D_i$  is the water depth and  $c_i$  is the dimensionless Chézy

140 coefficient, which can be calculated as (*Engelund and Fredsoe, 1982*):

$$c_i = 6 + 2.5 \log \left( \frac{1}{2.5} \frac{D_i}{d_{50}} \right), \quad (3)$$

141 with  $d_{50}$  indicating the median grain size.

142 Similarly, the volumetric sediment flux is computed as:

$$Q_{s_i} = W_i \sqrt{g \Delta d_{50}^3} \Phi \left( \theta_i, \frac{D_i}{d_{50}} \right), \quad \theta_i = \frac{S_i D_i}{\Delta d_{50}}, \quad (4)$$

143 where  $\Delta$  is the relative submerged density of the sediment,  $\theta_i$  is the Shields stress and  $\Phi$  is a  
144 function given by the sediment transport formula. Specifically, we used the *Parker* (1990) formula  
145 for gravel bed channels and the *Engelund and Hansen* (1967) formula for sand bed cases.

146 The free character of the bifurcation manifests itself in the symmetrical configuration of up-  
147 stream and downstream channels, which determines water and sediment fluxes that enter and exit  
148 the cells (Figures 2b and 2c). First, the input fluxes  $Q_i^{IN}$  and  $Q_{s_i}^{IN}$  that are delivered by the  
149 upstream channel into the node cells are uniform. Second, the absence of slope advantage (i.e.  
150  $S_b = S_c$ ) leads to the same water and sediment rating curves for the two bifurcates. Therefore,  
151 possible asymmetries of the output fluxes are not driven by the upstream/downstream conditions  
152 but can only derive from an uneven redistribution by the bifurcation node.

## 153 2.2 The forced bifurcation

154 Different forcing effects can be further incorporated in the free bifurcation model, to increase its  
155 ability of the model to represent real bifurcation configurations. The key to model those effects  
156 is to act on the upstream and boundary conditions imposed at the node cells, which practically  
157 implies considering non-uniform water and sediment fluxes entering the two node cells, and/or  
158 imposing different water and sediment rating curves for the two bifurcates. Such an approach has  
159 been already exploited by *Bertoldi et al.* (2009) when modelling how bifurcations dynamics can  
160 be affected by migrating bars, which were schematised as periodic temporal oscillations of water  
161 and sediment fluxes delivered to the node cells. Here we consider two different forcing effects: (i)



162 a downstream slope advantage of one bifurcate with respect to the other one and (ii) the presence  
 163 of a curved upstream channel.

164 A downstream slope advantage increases the probability for an unbalanced water and sediment  
 165 flux towards the “advantaged” distributary. This effect can be taken into account by setting  
 166 different values of  $S_b$  and  $S_c$  in Equations (2) and (4). This breaks the symmetry in the downstream  
 167 rating curves, even if the other geometrical parameters remain equal between the two downstream  
 168 branches. We quantify the slope advantage through the following parameter:

$$\Delta S = \frac{S_b - S_c}{S_b + S_c}, \quad (5)$$

169 with positive values of  $\Delta S$  indicating that the outer bend bifurcate (Channel  $b$  of Figure 2a) is  
 170 steeper than the inner bend bifurcate (Channel  $c$ ).

171 We model the presence of an upstream bend (Channel  $a$ ) feeding the bifurcation as does a  
 172 channel with constant radius of curvature  $R$ . The curvature of the main channel leads to the  
 173 formation of a spiral flow (Figure 3a), which in turn produces a shear stress in the transverse  
 174 direction. Therefore, the bottom stress ends up being deflected by an angle  $\phi_\tau$ , which can be  
 175 computed as (*Struiksmma et al.*, 1985):

$$\tan(\phi_\tau) = -A \frac{D}{R}, \quad (6)$$

176 where  $D$  is the local water depth and  $A$  is the coefficient that defines the intensity of the secondary  
 177 flow, given by:

$$A = \frac{2}{\kappa^2} \left( 1 - \frac{1}{\kappa c} \right) \quad (7)$$

178 with  $\kappa = 0.4$  indicating the Von Karman constant.

179 In the region where the flow is fully developed (i.e., far enough from the bend entrance),  
 180 the flow characteristics do not vary along the channel, and the depth-averaged velocity is purely  
 181 longitudinal. In these conditions, the deflection of the bed shear stress is compensated by a

182 transverse gradient of the bed elevation (see Figure 3a) that is given by:

$$\frac{d\eta}{dy} = \frac{\sqrt{\theta}}{r} \tan(\phi_\tau), \quad (8)$$

183 (for mathematical details see Appendix A), which in turn generates non-uniform transverse profiles  
 184 of water depth, longitudinal velocity and shear stress. Consequently, water and sediment fluxes  
 185 feeding the two cells are not uniform but are mainly delivered towards the cell positioned at the  
 186 outer bend (Cell B of Figure 3b).

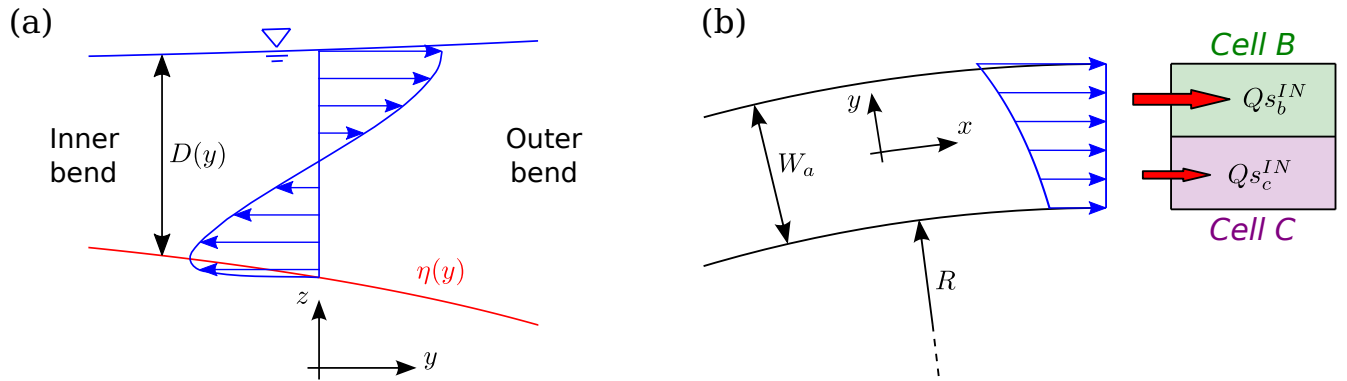


Figure 3: Illustration of the secondary flow solution in the upstream channel: (a) cross-sectional view, indicating the vertical profile of the transverse velocity (arrows), and the transverse profiles of bed elevation and water depth; (b) planimetric view, with the transverse velocity profile (arrows) and the associated sediment fluxes entering the cells ( $Qs_b^{IN}$  and  $Qs_c^{IN}$ ).

187 Furthermore, as suggested by *Kleinhans et al.* (2008) the deviation of the bed shear stress  
 188 given by Equation (6) is also active within the cells, so that the nodal point relation (1) needs to  
 189 be extended as follows:

$$\underbrace{\frac{Qs_y}{\alpha Qs_a}}_{\text{sediment flux direction}} = \underbrace{\frac{Q_y}{\alpha Q_a}}_{\text{velocity direction}} - \underbrace{\frac{2r}{\sqrt{\theta_a}} \frac{\eta_b - \eta_c}{W_b + W_c}}_{\text{gravitational effect}} - \underbrace{A \frac{D_a}{R}}_{\text{spiral flow effect}}, \quad (9)$$

190 where  $D_a$  and  $\theta_a$  are the average values of water depth and Shields stress in the upstream Channel  
 191  $a$ .

192 The above formulation is generally suitable for modelling bifurcations with arbitrary channel  
 193 widths. However, for the purpose of analysing the interaction between the different mechanisms,  
 194 also in comparison with previous works (e.g., *Bolla Pittaluga et al.*, 2015), we restrict our attention

195 to the basic case where both the bifurcates have half the width of the main channel ( $W_b = W_c =$   
 196  $W_a/2$ ).

### 197 **3 Results**

198 The model solution can be expressed as a function of a few dimensionless parameters. First,  
 199 the solution depends on the reference conditions, which are defined as the uniform flow and  
 200 sediment transport in a straight channel with same slope, width and discharge of the main channel.  
 201 Specifically, we need to prescribe three main parameters, namely the aspect ratio, the Shields stress  
 202 and the relative roughness:

$$\beta_0 = \frac{1}{2} \frac{W_a}{D_0}, \quad \theta_0 = \frac{S_a D_0}{\Delta d_{50}}, \quad d_{s0} = \frac{d_{50}}{D_0}, \quad (10)$$

203 where zero subscript (e.g.,  $D_0$ ) indicates the reference conditions.

204 Second, the solution depends on the intensity of the forcing effects, which is specified through  
 205 the normalized curvature  $W_a/R$  and the slope advantage  $\Delta S$ .

206 In the following, we analyse the model outputs in terms of discharge asymmetry (*Bertoldi*  
 207 *et al.*, 2009), which can be taken as a representative indicator of the bifurcation response:

$$\Delta Q = \frac{Q_b - Q_c}{Q_a}, \quad (11)$$

208 which may range from  $-1$  (no flow in Channel  $b$ ) to  $+1$  (no flow in Channel  $c$ ), with  $\Delta Q = 0$   
 209 indicating balanced bifurcations.

#### 210 **3.1 The free bifurcation**

211 The free bifurcation configuration is made by three straight channels without any slope advantage  
 212 nor width or angle asymmetry, thus without external effects that may force an unbalanced config-  
 213 uration. In this condition the intuitive expectation would be a symmetrical bifurcation response,  
 214 with an even distribution of downstream water and sediment fluxes. As illustrated in Figure 4,

215 the balanced configuration ( $\Delta Q = 0$ ) is indeed an equilibrium solution of the system. However,  
 216 for relatively high values of the aspect ratio the balanced configuration becomes unstable, and one  
 217 of the channels, indifferently, tends to dominate.

218 As highlighted by *Bolla Pittaluga et al.* (2003) this type of instability of the symmetric equilib-  
 219 rium solution does not necessarily lead to a complete closure of one branch, but new, unbalanced  
 220 and stable equilibrium states are possible. In Figure 4, this is represented by the formation of a  
 221 so called “pitchfork bifurcation” (e.g., *Wiggins*, 2003) in the equilibrium diagram, which occurs  
 222 at  $\beta_0$  near 13.5. The two unbalanced equilibrium configurations are physically sustained by the  
 223 formation of an inlet step, i.e. a localized steep reach at the head of the largest flow-carrying bifur-  
 224 cate (*Bertoldi et al.*, 2009), which steers the sediment flux and thus satisfies the balance between  
 225 sediment supply and transport capacity of the bifurcates.

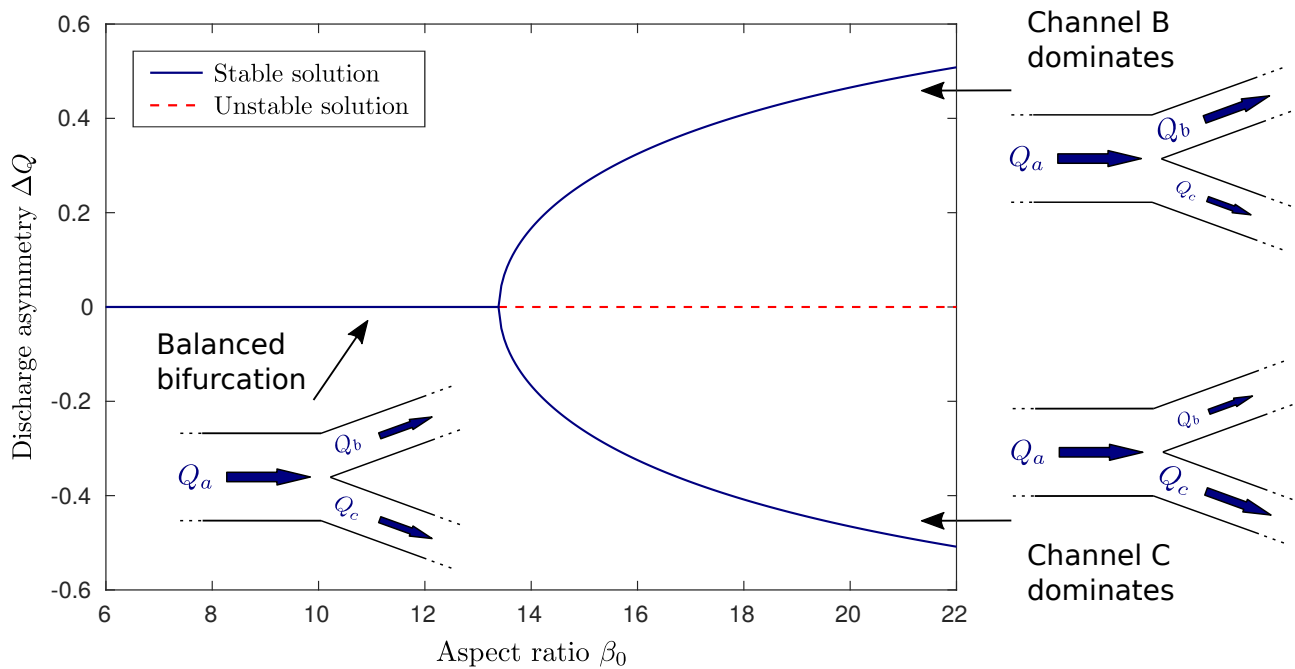


Figure 4: Equilibrium solutions of a free bifurcation (i.e. straight channel with no slope advantage) according to the two-cell model. Solid lines indicates stable solutions, while the dashed line represents an unstable equilibrium configuration. Parameters are  $\theta_0 = 0.1$ ,  $d_{s0} = 0.02$ ,  $r = 0.5$ ; the *Parker* (1990) transport formula is used.

226 The critical point at which the pitchfork bifurcation appears is determined through a linear  
 227 stability analysis (*Bolla Pittaluga et al.*, 2015), whose result can be expressed in the following

228 general form:

$$\beta_C = \frac{r\alpha}{\sqrt{\theta_0}} \frac{4}{\Phi_D + \Phi_T - (3/2 + c_D)}, \quad (12)$$

229 whose coefficients are defined as:

$$c_D := \frac{D_0}{c_0} \frac{\partial c}{\partial D} \Big|_{D_0}, \quad \Phi_D := \frac{D_0}{\Phi_0} \frac{\partial \Phi}{\partial D} \Big|_{D_0, \theta_0}, \quad \Phi_T := \frac{\theta_0}{\Phi_0} \frac{\partial \Phi}{\partial \theta} \Big|_{D_0, \theta_0}, \quad (13)$$

230 and represent the sensitivity of Chézy coefficient and of the dimensionless sediment transport rate  
231 to variations of water depth and Shields stress. The algebraic expressions of the coefficients  $c_D$ ,  
232  $\Phi_D$  and  $\Phi_T$  for the used formulae of *Parker* (1990) and of *Engelund and Hansen* (1967), as well  
233 as for the classical relation of *Meyer-Peter and Muller* (1948), are reported in Appendix B for  
234 the sake of clarity. Equation (12) represents a generalization of the formula proposed by *Bolla*  
235 *Pittaluga et al.* (2015) for arbitrary transport and friction formulae.

236 According to Equation (12), the critical aspect ratio is directly proportional to the cell length  
237 represented by  $\alpha$ . In a 1D formulation, the parameter  $\alpha$  needs to be empirically calibrated,  
238 resulting in rather different literature values, ranging from 1 (*Bolla Pittaluga et al.*, 2003) to  
239 6 (*Bertoldi and Tubino*, 2007). This limitation has been solved by *Redolfi et al.* (2016), who  
240 developed an analytical linear solution of the fully 2D problem; in that formulation, the length of  
241 the upstream cells is resolved by the model itself, so that no specific calibration is needed.

242 The analysis of *Redolfi et al.* (2016) demonstrated that the emergence of an unbalanced solution  
243 in a free bifurcation depends on the formation of an upstream steady bar, which occurs when the  
244 bifurcation is able to exert a morphodynamic influence in the upstream direction (see Figure  
245 5). As theoretically derived by *Zolezzi and Seminara* (2001) and experimentally observed by  
246 *Zolezzi et al.* (2005) any fixed geometrical disturbance can produce a permanent upstream bed  
247 deformation, usually taking the form of a steady bar, when the channel is wide and shallow enough  
248 for the aspect ratio of the main channel to exceed the resonant threshold,  $\beta_R$ , as originally defined  
249 in the theory of regular meanders by *Blondeaux and Seminara* (1985). Therefore, under super-  
250 resonant conditions ( $\beta_0 > \beta_R$ ) the bifurcation node - as a fixed geometrical disturbance - can  
251 trigger such an upstream morphodynamic influence. This is essentially the physical mechanism

252 behind the mathematical instability of the balanced equilibrium solution, which therefore makes  
 253 a free bifurcation unbalanced.

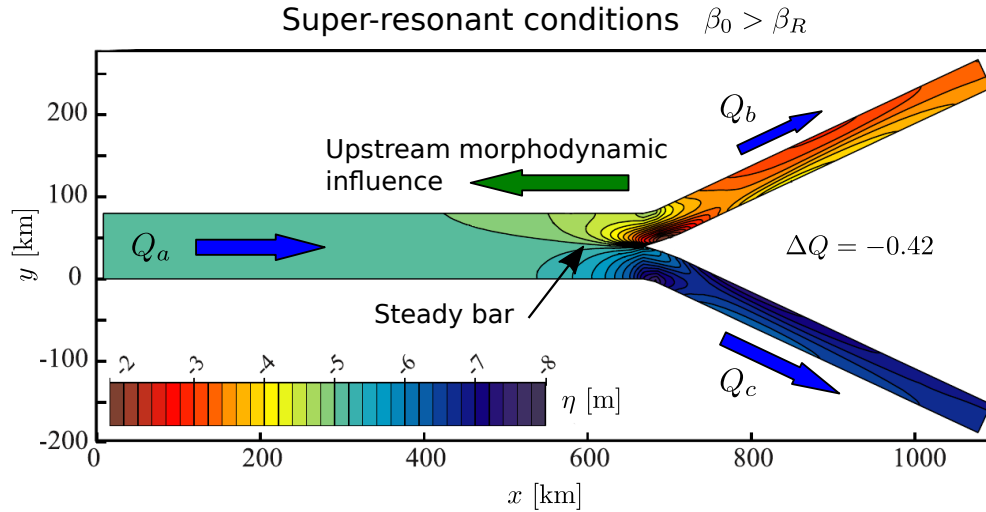


Figure 5: Map of bed elevation and water distribution in a free bifurcation from the numerical simulations of *Edmonds and Slingerland* (2008), adapted from their Figure 5b. The equilibrium configuration is made unbalanced by the formation of an upstream steady bar, which deviates most water and sediment fluxes towards the right bifurcate. According to *Redolfi et al.* (2016) this is an effect of the upstream morphodynamic influence exerted by the bifurcation node, which occurs when the aspect ratio of the upstream channel  $\beta_0$  exceeds the resonant threshold  $\beta_R$ .

254 The computation of the resonant aspect ratio requires the solution of a fourth-order polynomial,  
 255 which can be readily obtained using the available Matlab code (see Acknowledgements Section).  
 256 The resulting values for gravel bed and sand bed river channels as a function of the relevant  
 257 dimensionless parameters are reported in Figures 6a and 6b, respectively. For sand bed rivers  
 258 the Chézy coefficient is independently fixed, rather than derived from Equation (3), to account  
 259 for the higher drag exerted by bedforms, also consistently with previous applications (*Edmonds*  
 260 *and Slingerland*, 2008). In gravel bed channels  $\beta_R$  increases with both the Chézy coefficient and  
 261 the Shields stress, which explains the tendency of bifurcations to stabilize when increasing  $\theta_0$   
 262 (*Bolla Pittaluga et al.*, 2015). Conversely, in sand bed channels the resonant threshold tends to  
 263 decrease with the Shields stress, which explains the opposite effect of  $\theta_0$  observed by *Edmonds*  
 264 *and Slingerland* (2008). Consistently with *Bolla Pittaluga et al.* (2015) the different behaviour of  
 265 sand bed and gravel bed channels is related to the different response of the dimensionless sediment  
 266 transport rate to variations of the Shields stress (which depends on the transport formula) rather

Table 1: List of datasets used to evaluate the resonance criterion for bifurcation instability.

Dataset	Method	Bed material	# of cases	$\beta_0$	$\theta_0$
<i>Bertoldi and Tubino (2007)</i>	Laboratory	gravel	25	4.9 – 26.3	0.042 – 0.099
<i>Edmonds and Slingerland (2008)</i>	Numerical	sand	11	8	0.80 – 2.19
<i>Siviglia et al. (2013)</i>	Numerical	gravel	18	3.5 – 24.0	0.060 – 0.200
<i>Zolezzi et al. (2006)</i>	Field	gravel	6	9.5 – 14.5	0.053 – 0.088
<i>Bolla Pittaluga et al. (2015)</i>	Field	sand	11	16.9 – 77.1	0.30 – 1.16

267 than an effect of a gradient in the water surface elevation near the bifurcation, as suggested by  
 268 *Edmonds and Slingerland (2008)*.

269 Alternatively, the resonant aspect ratio can be calculated though the approximate expression  
 270 by *Camporeale et al. (2007)*:

$$\beta_R = \frac{\pi}{2\sqrt{2}} \frac{c_0\sqrt{r}}{\theta_0^{1/4}} \frac{1}{\sqrt{\Phi_D + \Phi_T - (3/2 + c_D)}}, \quad (14)$$

271 which provides rather accurate estimates of  $\beta_R$  for sand bed channels, while it gives slightly  
 272 underestimated values for gravel bed cases (up to  $-13\%$  for the range of parameters in Figure 6a).

273 The resonant threshold provides a simple criterion to determine if a free bifurcation remains  
 274 balanced or tends to evolve towards unbalanced states. To test this criterion we used the lit-  
 275 erature datasets listed in Table 1, which include gravel and sand bifurcations measured in the  
 276 field, modelled numerically and reproduced in laboratory-scale physical models. For each of the  
 277 71 bifurcations the different authors provided observation of their balanced/unbalanced state and  
 278 the basic flow parameters, which were used to compute the resonant threshold and the parameter  
 279  $(\beta_0 - \beta_R)/\beta_R$  representing the relative distance to resonance. We set  $r = 0.5$  for all cases except  
 280 for the *Edmonds and Slingerland (2008)* experiments, for which an equivalent  $r \simeq 0.35$  value was  
 281 needed to match the default  $\alpha_{bn} = 1.5$  value of their Delft3D formulation (e.g., *Lesser et al., 2004*).  
 282 Results reported in Figures 6c and 6d show that balanced bifurcations (closed markers) tend to  
 283 stay below the dashed line (i.e. sub-resonant conditions), while all the unbalanced bifurcations  
 284 (open markers) are located above the dashed line (i.e. super-resonant conditions), independently  
 285 of the Shields stress. It is worth noting that the resonant criterion also captures the numerical  
 286 results of *Edmonds and Slingerland (2008)*, who demonstrated that balanced solutions in sand bed  
 287 channels tends to become unstable with increasing  $\theta_0$ . The above analysis confirms that the reso-

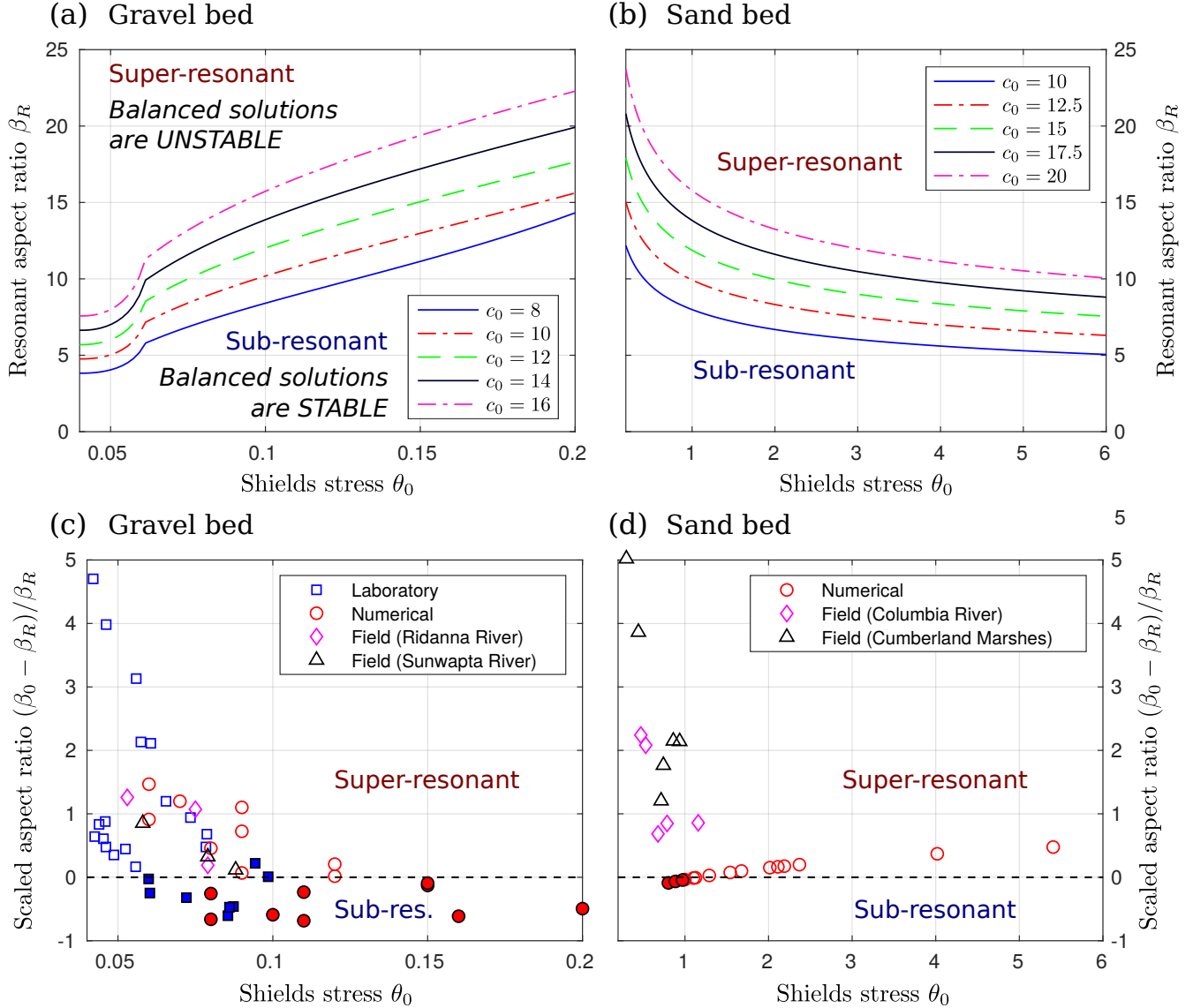


Figure 6: (a) and (b) Resonant aspect ratio  $\beta_R$  for gravel and sand bed channels as a function of Shields stress and Chézy coefficient. Under sub-resonant conditions (i.e.  $\beta_0 < \beta_R$ ) the balanced bifurcation configuration is stable, while in super-resonant channels ( $\beta_0 > \beta_R$ ) the instability mechanism makes the bifurcation unbalanced. (c) and (d) Observations of the balanced (close markers) or unbalanced (open markers) state of the bifurcation as a function of Shields stress and relative distance from the resonant threshold (scaled aspect ratio), for each of the 71 bifurcations listed in Table 1.



288 nant threshold correctly predicts stability of both gravel and sand bed bifurcations, with the key  
 289 advantage of avoiding the need of calibrating a specific parameter like the  $\alpha$  required by previous  
 290 theoretical models (e.g., *Bolla Pittaluga et al.*, 2003, 2015).

291 The value of  $\alpha$  that makes the nonlinear two-cell model consistent with the 2D theory can  
 292 be determined by simply setting  $\beta_C = \beta_R$  in Equation (12). Results reported in Figure 7 show  
 293 a significant dependence of  $\alpha$  on the reference conditions ( $\theta_0$  and  $c_0$ ), which explains the large  
 294 variability emerging in the literature. We notice that this estimate is strictly valid in the neighbour  
 295 of the instability threshold, while for larger  $\beta$  it provides an upper limit of the optimal value for  
 296 predicting the discharge asymmetry, as suggested by both laboratory observations and theoretical  
 297 considerations (*Bertoldi and Tubino*, 2007; *Redolfi et al.*, 2016).

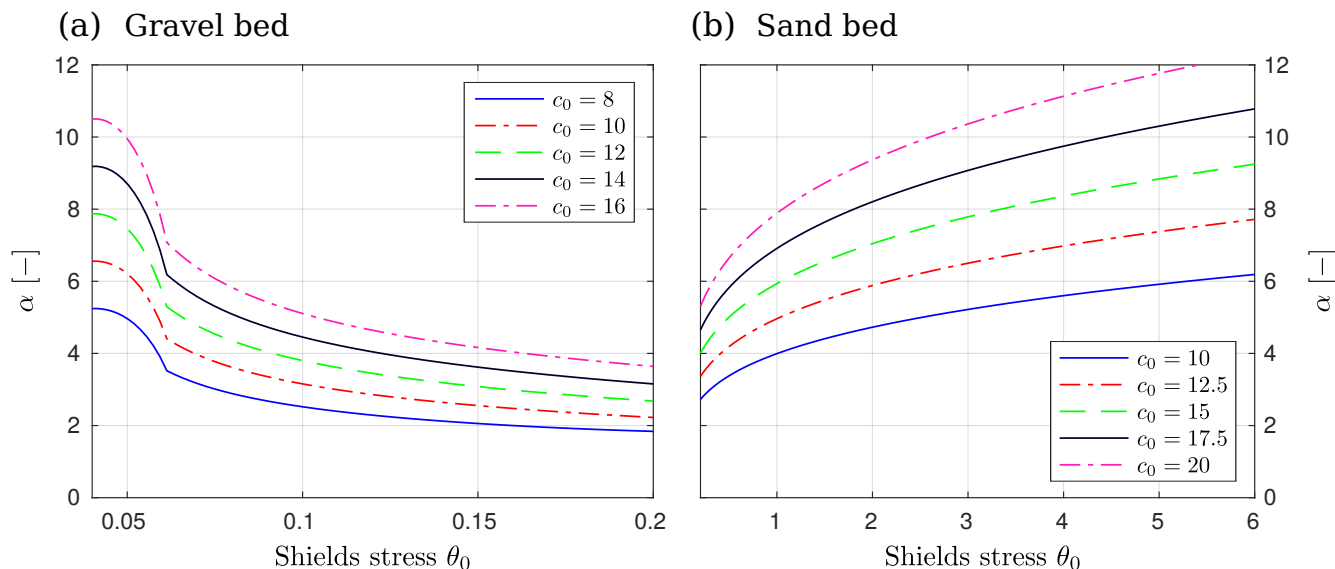


Figure 7: Values of the parameter  $\alpha$  that make the two-cell model consistent with the linear 2D theory of *Redolfi et al.* (2016): (a) gravel bed channels, (b) sand bed channels.

298 Data of Table 1 include field measurements of natural bifurcations, which are not necessarily  
 299 free. In this case the observed asymmetry may be not fully ascribed to the free instability mecha-  
 300 nism but it may also be enhanced by the presence of the external forcings. The analysis of forcing  
 301 effects and their interaction with the free instability mechanism is the main subject of the next  
 302 section.

## 3.2 The forced bifurcation

Natural bifurcations are rarely free because of a number of forcing effects, including curvature of the main channel, different bifurcation angles, slope advantages, migration of bars, presence of obstacles, differential downstream sedimentation (e.g. *Van der Mark and Mosselman, 2013; van Dijk et al., 2014; Le et al., 2018b,a; Salter et al., 2018*).

In the presence of a forcing effect, for example a curvature of the main channel, the equilibrium diagram of Figure 4 changes its topology. Specifically, as illustrated in Figure 8a, the equilibrium solution at relatively low values of  $\beta_0$  is not balanced (i.e.  $\Delta Q = 0$ ) and as expected more water is flowing towards the outer bend. When  $\beta_0$  increases, the effect of the channel curvature tends to be amplified by the bifurcation, resulting in a more and more unbalanced configuration. However, at a given  $\beta$  value two additional equilibrium solutions form (a so called “imperfect pitchfork bifurcation”, see for example *Golubitsky and Schaeffer, 1979*). One of them is unstable (dashed line in Figure 8a), while the more unbalanced solution is stable. This suggests the possibility for the bifurcation to attain a different, stable equilibrium point, where most of water and sediment fluxes are deviated towards the inner bend bifurcate.

The behaviour of the equilibrium solutions for different values of the dimensionless channel curvature  $W_a/R$  is illustrated in Figure 8b. When  $W_a/R = 0$  (straight channel) we obtain again the solution of Figure 4, here represented in terms of the distance from the resonant point, so that the pitchfork “bifurcation” appears at  $(\beta_0 - \beta_R)/\beta_R = 0$ . By analysing the effect of increasing curvature two relevant aspects emerge. First, the increase of the discharge asymmetry with channel curvature is significantly more pronounced at relatively small values of the channel aspect ratio (i.e. in the sub-resonant regime), where lines corresponding to different curvature values are more spaced apart, while at higher (i.e., super-resonant) aspect ratios the effect of curvature is minimal. Second, the value of the aspect ratio at which the second stable solution forms increases with channel curvature. For example, when  $W_a/R = 0.1$  an aspect ratio 50% higher than the resonant value is needed to allow for the existence of multiple stable solutions.

The possibility of obtaining multistable solutions depending on channel curvature and aspect ratio is better illustrated in Figure 9a. While under sub-resonant conditions the equilibrium

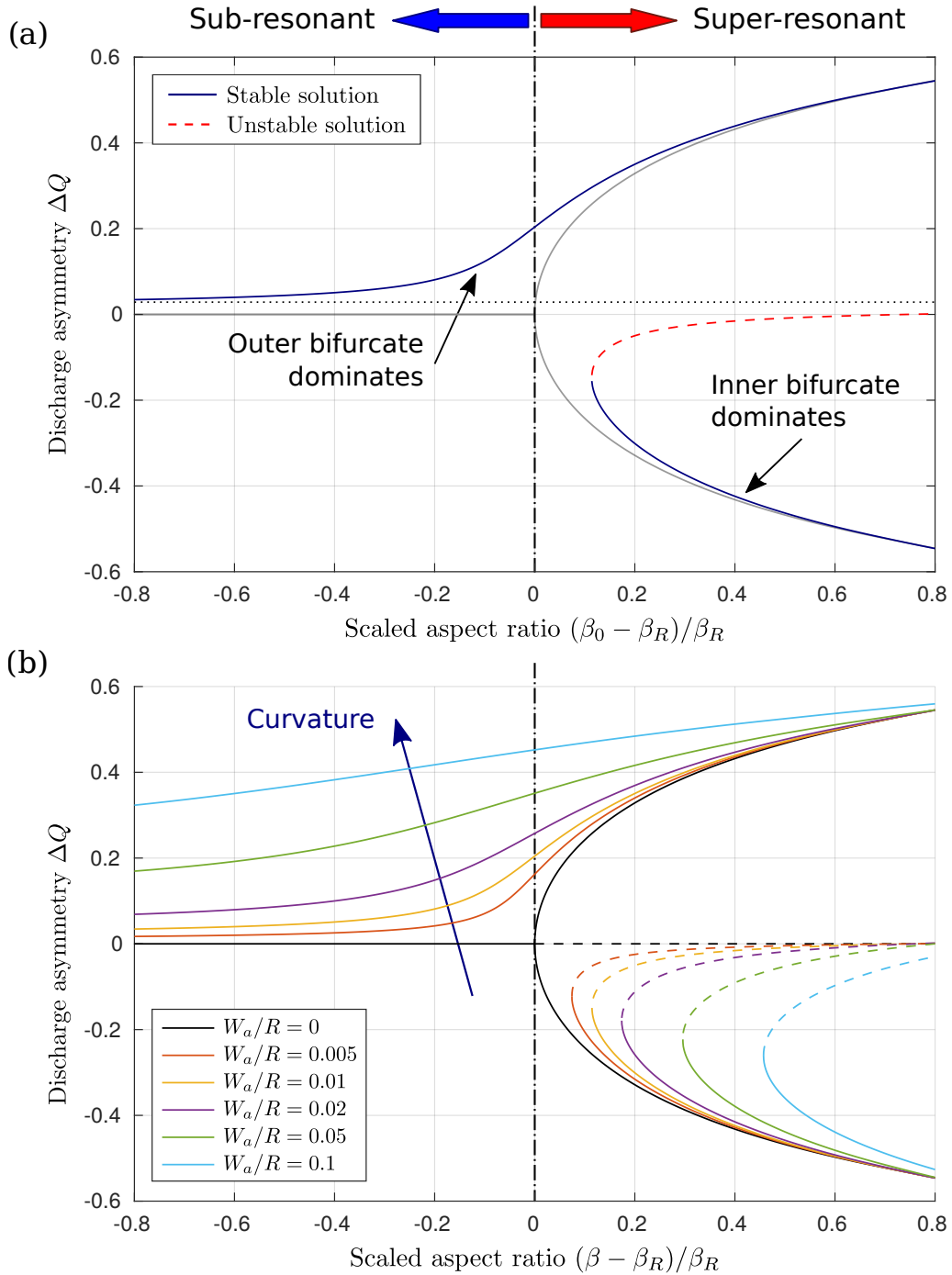


Figure 8: Stable (solid lines) and unstable (dashed lines) equilibrium solutions for a bifurcation with a curved upstream channel, as a function of the scaled aspect ratio. (a) Example with fixed curvature ( $W_a/R = 0.01$ ), where the dotted line indicates the discharge ratio at the cell entrance and the grey lines represent the reference, “free” solution. (b) Effect of increasing curvature values. The vertical dashed line separates the sub-resonant (left) from the super-resonant (right) region.

331 solution is unique, two stable equilibrium solutions exist in super-resonant conditions. However,  
 332 if the curvature is sufficiently large (depending on  $(\beta_0 - \beta_R)/\beta_R$ ) only the solution for which the  
 333 outer channel dominates is possible.

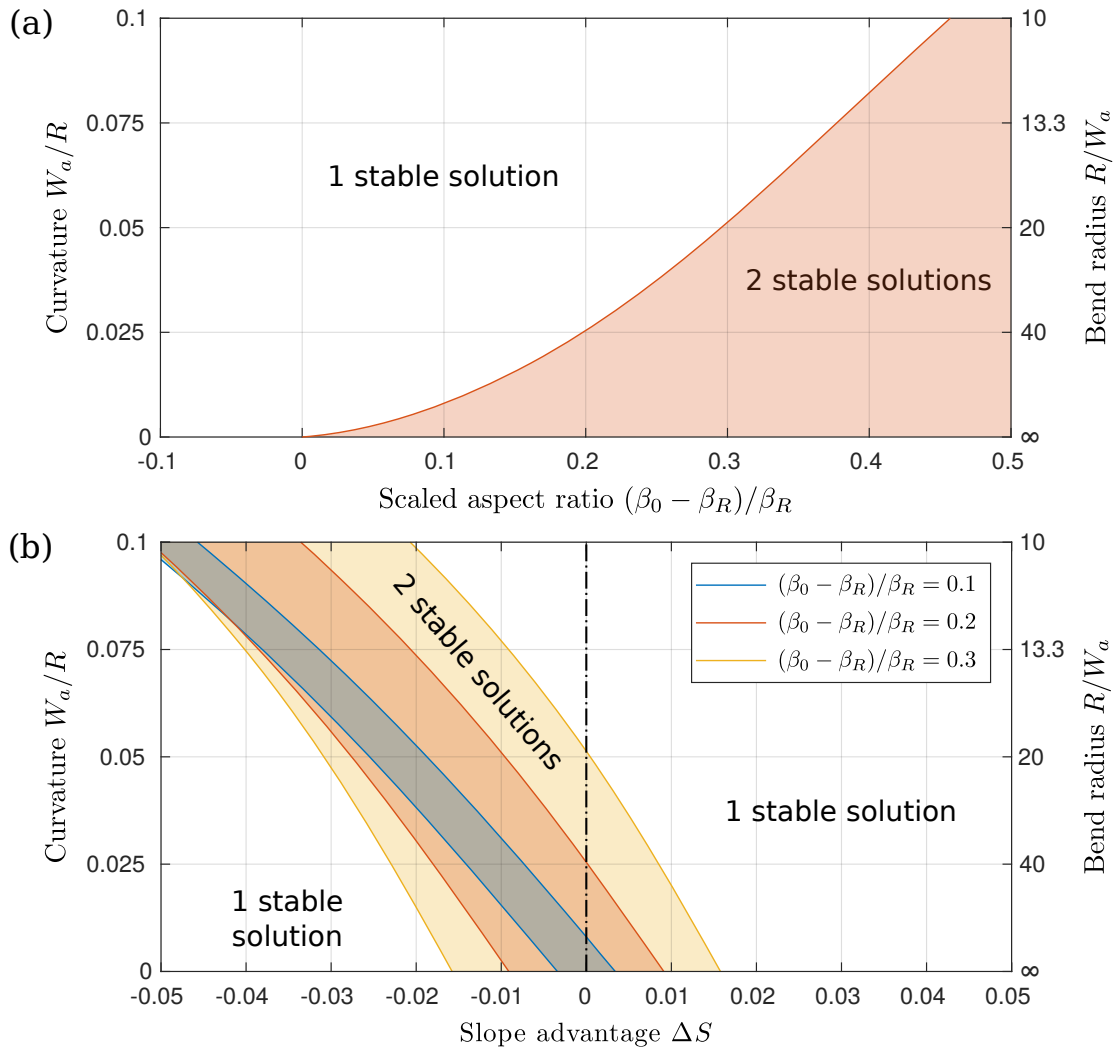


Figure 9: Stability diagram indicating regions where two stable equilibrium solutions exist depending on: (a) scaled aspect ratio and channel curvature (no slope advantage); (b) the combined effect of channel curvature and slope advantage, for different values of the scaled aspect ratio.

334 The above depicted scenario is characteristic of imperfect systems, and turns out to be similar  
 335 when analysing different kind of forcings. Here we do not specifically report on the effect of the  
 336 slope advantage but we directly focus on the more interesting analysis of its interaction with the  
 337 curvature of the upstream channel.

338 In some cases the effect of main channel curvature can be compensated by a slope advantage  
 339 that tends to steer water and sediment flows towards the steeper inner bend bifurcate (e.g., Klein-

340 *hans et al., 2008; van Dijk et al., 2014*). Analysis of the combined effect of the different forcings  
341 on the discharge asymmetry gives the results illustrated in Figure 10a, which confirms that for a  
342 sub-resonant bifurcation a channel curvature can be compensated by a gradient advantage. When  
343  $\Delta S = -0.01$  the discharge asymmetry is the same as the upstream asymmetry independently of  
344  $\beta_0$ , while for higher slope advantages the bifurcation tends to distribute water towards the inner  
345 bend channel, in a greater proportion when  $\beta_0$  increases. However, the scenario dramatically  
346 changes when the aspect ratio exceeds the resonant threshold (i.e. super-resonant conditions).  
347 In this case, equilibrium solutions are never balanced, with one of the two bifurcates becoming  
348 dominant for any combination of curvature and slope advantage. In Figure 10b one sees that un-  
349 der sub-resonant conditions the equilibrium  $\Delta Q$  varies smoothly with the slope advantages, while  
350 when  $\beta_0$  exceeds  $\beta_R$  sharp transitions and hysteresis are expected when varying  $\Delta S$ .

351 In general the discharge asymmetry depends on slope advantage and curvature as illustrated in  
352 Figure 11. Under sub-resonant conditions (Figure 11a) variations of  $\Delta Q$  are always smooth, and  
353 the effect of channel curvature can be always compensated by negative values of  $\Delta S$ . Conversely,  
354 under super-resonant conditions (Figure 11b) the bifurcation is never balanced, and there is a well-  
355 defined region (black oblique stripes) in the forcing parameters space where two stable solutions  
356 coexist. The width of such bi-stable region depends on the distance from the resonant point as  
357 depicted in Figure 9b.

358 It is important to remark that all our diagrams have been obtained by considering fixed values  
359 of relative roughness ( $d_{s0} = 0.02$ ), Shields stress ( $\theta_0 = 0.1$ ) and *Ikeda* (1982) coefficient ( $r = 0.5$ ),  
360 and the same transport (*Parker*, 1990) and friction (Equation (3)) formulae. Nevertheless, from a  
361 qualitative point of view, model results, and therefore their interpretation, are fully independent  
362 of the specific choice of flow parameters values and closure relations for sediment transport.

## 363 4 Discussion

364 The present work has built on previous analyses to propose a theoretical framework for river bifur-  
365 cations within the context of 1D morphodynamic modelling that accounts for key 2D ingredients  
366 at the entrance of the bifurcation node and in the fluxes delivered by the upstream channel.

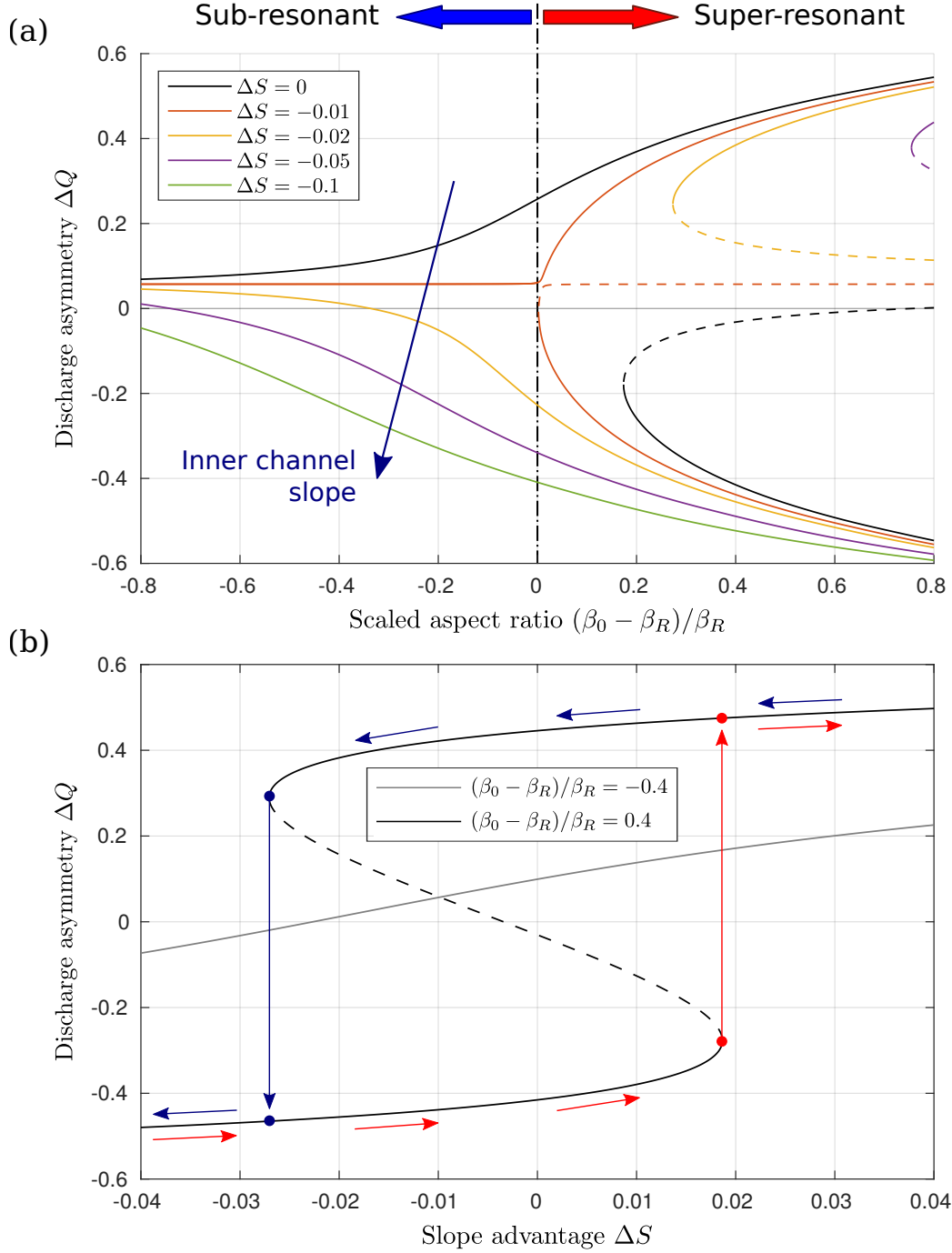


Figure 10: Effect of the slope advantage on a curved ( $W_a/R = 0.02$ ) bifurcation. (a) Equilibrium solutions as a function of the aspect ratio  $\beta_0$ . (b) Equilibrium solutions as a function of the slope advantage under sub-resonant (grey line) and super-resonant (black lines) conditions. Solid and dashed lines indicate stable and unstable solutions respectively, while arrows indicate possible trajectories when increasing (red arrows) or decreasing (blue arrows)  $\Delta S$ .

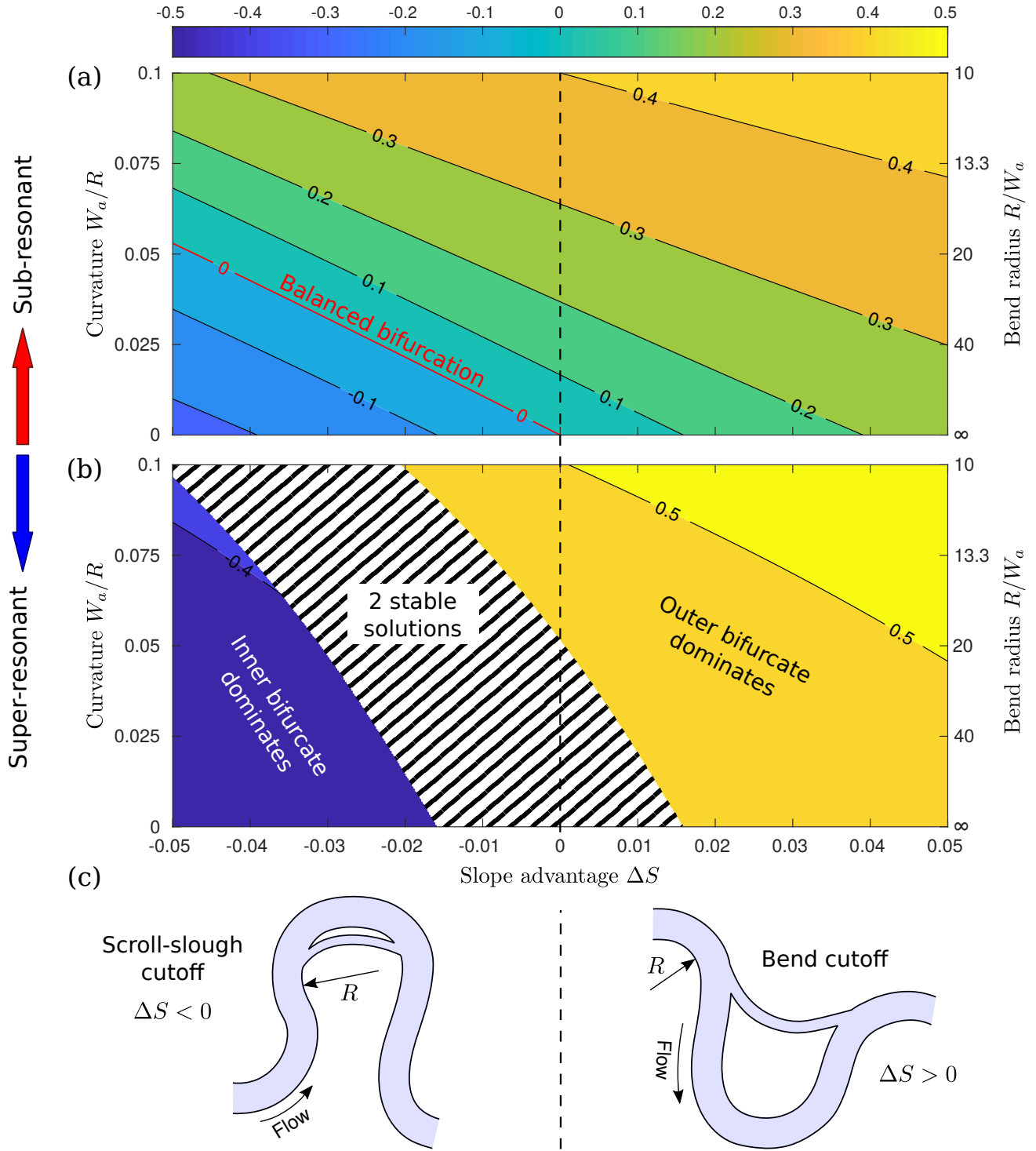


Figure 11: Discharge asymmetry as a function of curvature and slope asymmetry: (a) sub-resonant conditions ( $(\beta_0 - \beta_R)/\beta_R = -0.3$ ); (b) super-resonant conditions ( $(\beta_0 - \beta_R)/\beta_R = 0.3$ ), with black oblique stripes indicating the region where two stable solutions exists. (c) example of different slope advantages in meanders chute cutoff. Left: steeper inner channel ( $\Delta S < 0$ ); right: steeper outer channel ( $\Delta S > 0$ ).

367 Here we discuss (i) the main implications of our findings and the potential of the proposed  
368 approach for the interpretation of bifurcation dynamics, as it emerges from both observations and  
369 modelling; (ii) the significance of the equilibrium analysis for time-dependent processes; (iii) the  
370 need to clarify the specific use of the wording “instability” when addressing bifurcation dynamics,  
371 in the light of our findings and in the context of previous studies; (iv) applicability and limitations  
372 of our approach.

373

374 *Enhanced insight on bifurcation morphodynamics*

375 The core of the model lies in incorporating in the 1D scheme of *Bolla Pittaluga et al. (2003)*  
376 (i) the resonant aspect ratio as threshold for bifurcation stability (*Redolfi et al., 2016*) and (ii)  
377 the effect of the forcing factors, through a proper modelling of the water and sediment fluxes  
378 delivered from the upstream channel and accepted by the downstream bifurcates. These fluxes  
379 are laterally symmetrical in the case of a purely free bifurcation, while the opposite occurs when  
380 adding forcing effects, which are almost invariably observed in real settings. Among the broad  
381 variety of forcing factors that characterize natural river bifurcations, here we addressed the isolated  
382 and the combined effect of an upstream channel curvature and a gradient advantage between the  
383 downstream branches.

384 A first important insight allowed by the proposed approach is the confirmation of the key role  
385 of the resonant aspect ratio on bifurcation behaviour, and an in-depth quantitative understanding  
386 of how the bifurcation response depends on the relative distance of the channel-forming aspect  
387 ratio value from such resonant threshold. This is supported with an analysis of an unprecedented  
388 number of laboratory, numerical and field data, for both gravel-bed and sand bed streams. The  
389 stability criterion based on the resonant threshold explains the loss of stability with increasing  
390 Shields stress of balanced sand bed bifurcations observed by *Edmonds and Slingerland (2008)*,  
391 which is simply the consequence of adopting different transport and friction formulae. Compared  
392 with previous stability criteria, the analysis based on resonance offers the key advantage that it  
393 does not require the calibration of a specific parameter like the  $k$  exponent of *Wang et al. (1995)*  
394 or the  $\alpha$  length parameter of *Bolla Pittaluga et al. (2003, 2015)*.



395 Interestingly, the role of the free instability mechanism is not limited to ideal, geometrically  
396 symmetric bifurcations with symmetrical boundary conditions, but it is also a key controlling  
397 factor for complex, forced bifurcations. Consequently, also the response of bifurcation to the  
398 external forcings highly depends on channel conditions with respect to resonance. Under sub-  
399 resonant conditions, the bifurcation behaviour is relatively simple, as it is perfectly balanced for  
400 free, symmetrical bifurcations and mostly dominated by the forcing effects when they are present.  
401 On the contrary, under super resonant conditions balanced equilibrium configurations are never  
402 stable, so that the bifurcation always tends to highly asymmetric equilibrium states. Here, multiple  
403 stable solutions are possible, including counter-intuitive configurations where the inner bifurcate  
404 prevails, which suggests the possibility of complete shifts and hysteresis in the bifurcation response  
405 to changing conditions (*Scheffer et al.*, 2001).

406 The whole picture yields a clear, physically-based key to interpreting results of field observa-  
407 tions and numerical models, which at times displayed behaviours that could not be given a fully  
408 exhaustive explanation. An example is provided by the result of *Kleinhans et al.* (2008), based on  
409 a three-dimensional model of a curved bifurcation with different channel gradients. These results  
410 revealed a “dramatic effect” of the width to depth ratio on discharge distribution and overall bed  
411 morphology, with the bifurcation switching from a dominant inner-bend bifurcate to a dominant  
412 outer-bend bifurcate, which indicates that the bifurcation behaviour “bifurcates” at a certain  
413 width between  $W_a = 288$  m and 378 m (see Section 4.5 of *Kleinhans et al.*, 2008). By applying our  
414 proposed modelling framework, and using the same closure relation and flow conditions as in the  
415 numerical experiments, it turns out that the observed range of widths correspond to the transition  
416 from from sub-resonant (Figure 12a) to super-resonant (Figures 12b and 12c) conditions. This  
417 transition can explain the fairly different morphological evolution upstream the bifurcation: under  
418 sub-resonant conditions the bifurcation does not significantly affect the upstream bed elevation  
419 (dashed line of Figure 12a), while under super-resonant conditions the upstream morphodynamic  
420 influence triggered by the bifurcation induces the formation of steady bars in the upstream channel  
421 (Figures 12b and 12c), which affect how discharge is downstream distributed.

422 Super-resonant conditions are not rare in nature, insofar as gravel bed rivers tends to behave

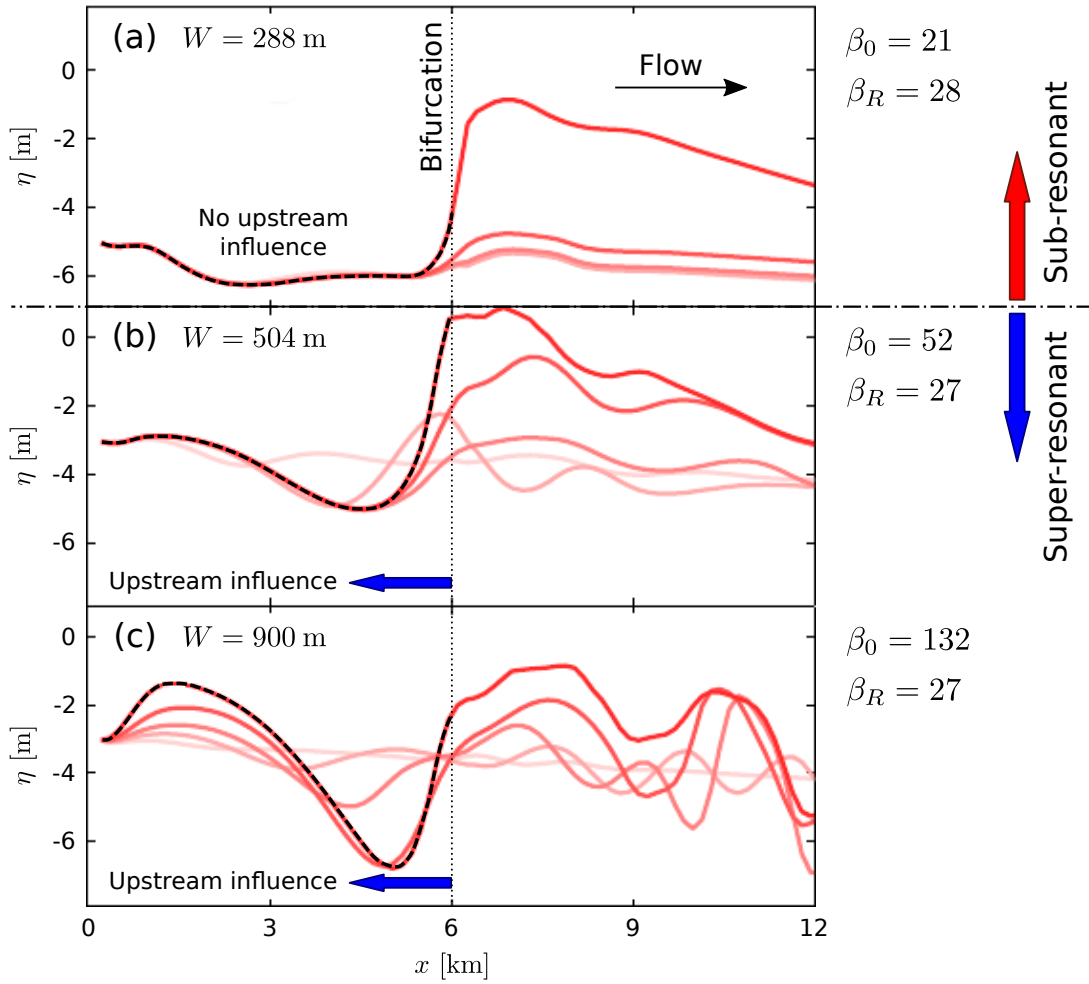


Figure 12: Profiles of bed elevation at the outer bank of a curved channel that bifurcates at  $x = 6$  km, according to the numerical simulations of *Kleinhans et al.* (2008), adapted from their Figure 12 (long bend series). (a) Sub-resonant conditions; (b) and (c) super-resonant conditions. Lines from light to dark indicate advancing time. The dashed line indicates the final bed profile upstream the bifurcation, which shows significant oscillations only when the upstream channel falls under super-resonant conditions.

423 super-resonantly, especially for near-threshold (i.e. low Shields stress) channels (*Zolezzi et al.*,  
424 2009). This confirms the tendency of balanced bifurcations to become unstable when the fixed  
425 bank hypothesis is released so that channels are free to reach their regime width (*Miori et al.*,  
426 2006).

427 When different forcing effects are simultaneously acting they can compensate themselves (e.g  
428 *Kleinhans et al.*, 2008; *van Dijk et al.*, 2014; *Kleinhans et al.*, 2013), leading to a nearly balanced  
429 configuration. For example a gradient advantage in a scroll-slough chute cutoff of a meander bend  
430 (Figure 11c) can balance the opposite effect of the channel curvature. However, this is possible  
431 only if the upstream channel is in sub-resonant conditions, so that the bifurcation is intrinsically  
432 stable. On the contrary, under super-resonant conditions the bifurcations tends to propagate its  
433 morphodynamic influence in the upstream direction, so that the discharge partition is always  
434 highly unbalanced, independently of the upstream and downstream conditions.

435 Similar results can be found when other kind of forcing effects are interacting with the free  
436 instability mechanism, as emerging in the analysis of *Bertoldi et al.* (2009) about the effect of  
437 downstream-migrating alternate bars on the bifurcation dynamics. In that context, different char-  
438 acteristic regimes have been identified depending on the channel aspect ratio with respect to a  
439 critical threshold. For relatively small  $\beta_0$  the bifurcation is essentially balanced with discharge  
440 oscillations around  $\Delta Q = 0$  caused by the passage of bars, while for higher  $\beta_0$  unbalanced states  
441 are observed. In this latter case the bifurcation can be either “bar perturbed” (small oscilla-  
442 tions around a stable unbalanced state) or “bar dominated” (frequent switching of the bifurcation  
443 between opposite, highly unbalanced states). A diagram similar to Figure 10b can be used to in-  
444 terpret the different scenarios: essentially balanced solutions occur under sub-resonant conditions,  
445 while super resonant conditions yield highly unbalanced solutions, which are “bar perturbed”  
446 when the variations of the forcing factor are relatively weak, or “bar dominated” when forcing  
447 effect is strong enough to make the solution jumping between opposite states.

448

449 *Quasi-equilibrium and temporal scales: the present work in a broader context*

450 Our analysis is focused on steady equilibrium configurations, where both upstream and down-

451 stream channels are considered in planimetric and altimetric equilibrium. Strictly speaking, this  
452 is rarely the case of natural bifurcation, because forcing effects are usually varying in time. Nev-  
453 ertheless, as long as their rate of change is slow as compared with the intrinsic time scale of the  
454 bifurcation, the response of the system can be studied as a sequence of quasi-equilibrium states.  
455 This allows us to interpret the action of downstream migrating bars, as well as the analogous  
456 effect of the migration of the upstream meander (*Kleinhans et al.*, 2011), by means of equilibrium  
457 diagrams like those of Figure 10.

458 Similarly, the quasi-steady analysis can be applied for interpreting the effect of downstream  
459 variations, provided they are comparatively slow. For example, in the depositional systems in-  
460 vestigated by *Salter et al.* (2018), the interaction between the bifurcation and the downstream  
461 bifurcates leads to autogenic temporal oscillations of channel slope and discharge asymmetry.  
462 This process evolves on a time scale that is proportional to the length of the downstream bifur-  
463 cates, which is usually much longer than the intrinsic time scale of the bifurcation evolution (see  
464 *Miori et al.*, 2006). Therefore, focusing on the local behaviour of the bifurcation node, such down-  
465 stream mechanisms can be considered as an external forcing effect, coherently with the definition  
466 adopted in the present work.

467 This provides a worthwhile example of how the definition of the forcing factors depends in  
468 general on the spatial and temporal scales under consideration. An analogous concept is at the  
469 core of classical theoretical studies on bar-bend interactions in river meanders (e.g., *Tubino and*  
470 *Seminara*, 1990), which pointed out how the dynamics of sediment bars inside meandering chan-  
471 nels depends on the interaction between the free instability mechanisms that causes spontaneous  
472 development of migrating bars, and the effect of the variable meander curvature. In general also  
473 the channel curvature is not fixed but changes in time as the meander develops. However, as long  
474 as the two mechanisms act at different time scales, the planform evolution being a much slower  
475 process, when focusing on bar dynamics the meander curvature can be considered as a fixed forcing  
476 factor.

477

478 *The meaning of “instability” within bifurcation dynamics*

479 The outcomes of this work also suggest revisiting the use of the key wording “instability”,  
480 which has been often used in previous studies of river bifurcation morphodynamics, though in  
481 many times with different meanings. “Instability” has been indeed used to indicate: (i) the sit-  
482 uation whereby an equilibrium bifurcation configuration is unstable; (ii) a systematic change of  
483 the discharge distribution over time (e.g., *Kleinhans et al.*, 2013); (iii) a bifurcation that evolves  
484 towards an highly unbalanced configuration and eventually produces the complete closure of one  
485 of the two bifurcates (e.g., *Burge*, 2006; *Le et al.*, 2018b). In this paper we have used “instability”  
486 in its mathematical meaning (i), thus indicating the mathematical instability of an equilibrium  
487 configuration (mathematical solution), which in itself could be either symmetrical or asymmetri-  
488 cal, and therefore may become inconsistent with meanings (ii) or (iii). Moreover, though meanings  
489 (ii) and (iii) might be interchangeable under some circumstances, this does not apply in general,  
490 and they may not be of help in disentangling the role of the free and of the forced bifurcation  
491 mechanisms when analysing a specific situation. For example, the instability of the balanced so-  
492 lution in the super-resonant regime does not necessarily lead to the closure of one bifurcate, but  
493 often leads to a stable, unbalanced configuration. Similarly, a partial or complete channel closure  
494 may be caused by a forcing factor rather than an instability of an equilibrium configuration, which  
495 in itself could be symmetrical or asymmetrical. This is, for instance, the case when a localized  
496 obstacle deviates the flux towards one preferred bifurcate (*Le et al.*, 2018b).

497

#### 498 *Applicability and limitations of the present approach*

499 In this paper we have adopted a local viewpoint of the bifurcation morphodynamics, which  
500 focuses on a tile of a complex mosaic of processes where several autogenic mechanisms interact  
501 at different spatial and temporal scales (e.g., in the case of bifurcations coupled with aggrading  
502 downstream channels or embedded in braided networks).

503 The methodological approach can be broadly applied to analyse river bifurcations in real  
504 settings. The key ingredient required by the two-cell model to account for the upstream forcings  
505 is the availability of suitable transverse distributions of flow and sediment transport to compute  
506 water and sediment fluxes that enter the bifurcation node. Our results refer to the simple case of a

507 relatively long channel of constant curvature, and are based on the assumption of fully developed  
508 flow, which is not satisfied in short bends and in general when the curvature is spatially varying, as  
509 in meandering channels. Extending the model to treat such complex configurations would require  
510 coupling the two-cell nodal point conditions with a sound model for flow and bed topography in  
511 meandering channels (e.g., *Zolezzi and Seminara, 2001*). This analysis is beyond the scope of the  
512 present paper; however, we may expect that in this case bifurcation stability will depend not only  
513 on local curvature, but also on the position of the bifurcation node with respect to the steady  
514 pattern of point bars forming in the upstream channel (*Le et al., 2018a*).

515 Further investigation is needed to understand to what extent the key mechanisms driving the  
516 bifurcation instability, and in particular the upstream morphodynamic influence, can be affected  
517 by processes that are often not reproduced by mathematical and physical models. Specifically,  
518 two fundamental processes would probably need more consideration in future research. The first  
519 is sediment sorting: despite some indications of a relatively weak effect of grain sorting on the  
520 stability of migrating bars (*Lanzoni and Tubino, 1999*), its role in determining the bifurcation  
521 stability is not clear, especially in gravel bed channels (*Burge, 2006*). The second process is  
522 suspended sediment transport, which is often dominant in large, multi-thread, sand bed rivers  
523 (*Szupiany et al., 2012*): when suspended load is the dominant mode of sediment transport the  
524 gravitational pull towards the deeper channel is probably weaker, so that the bifurcation may be  
525 even more unstable than currently predicted (*Kleinhans et al., 2006*).

## 526 **5 Conclusions**

527 The present work offers a viewpoint of river bifurcations as dynamical systems for which a distinct  
528 role of the free and forced responses can be identified. We propose a theoretical framework based  
529 on the 1D model with two-cell bifurcation node originally developed by *Bolla Pittaluga et al.*  
530 (2003), as extended by *Kleinhans et al.* (2008) to account for the curvature-driven secondary  
531 flow. Furthermore, we incorporate the key outcomes of the fully 2D analytical approach of *Redolfi*  
532 *et al.* (2016) within the classical 1D scheme for river bifurcations. Two main forcing factors are  
533 considered, the curvature of the upstream channel and a slope advantage of one of the bifurcates,

534 though the approach could be easily extended to account for other factors (e.g., the presence of a  
535 local obstacle upstream the bifurcation).

536 The key advantage of the proposed approach is its ability to clearly isolate the different free  
537 and forced mechanisms that may control the bifurcation dynamics in a complex setting, like that  
538 of real-world bifurcations, thus resulting in a suitable tool to gain clear insight in the analysis and  
539 interpretation of numerical model outcomes and of field observations. The key novel outcomes for  
540 bifurcation dynamics can be summarized in the following four items.

- 541 1. The bifurcation stability criterion based on the resonant aspect ratio threshold has been  
542 successfully tested against data of both gravel bed and sand bed channels, and it allows  
543 for capturing the opposite effects of Shields stress, which tend to promote more balanced  
544 bifurcations in gravel bed rivers and more unbalanced bifurcations in sand bed streams.  
545 This criterion can then be used for predicting the balanced/unbalanced character of free  
546 bifurcations, and it allows incorporating the fully-2D solution of *Redolfi et al.* (2016) within  
547 the classical 1D theory (*Wang et al.*, 1995; *Bolla Pittaluga et al.*, 2003) with no need to  
548 calibrate specific bifurcation parameters.
- 549 2. The role of the free instability mechanism is not limited to purely free bifurcations, but is  
550 also fundamental in the dynamics of the forced bifurcations that are more representative of  
551 real-world settings. Therefore, river bifurcations with super-resonant upstream channels are  
552 dominated by the free mechanism, characterized by multiple, highly unbalanced equilibrium  
553 configurations. This remarkable behaviour might lead to counter-intuitive outcomes, where  
554 for example water and sediment fluxes are mainly delivered towards the bifurcate located at  
555 the inner bank of a channel bend.
- 556 3. Analysis of the interaction between two of the most common forcing effects (slope advantage  
557 and curvature) allows us to quantify the parameters range where free and forcing effects  
558 cooperate or compete in determining the overall bifurcation dynamics. Under sub-resonant  
559 conditions, the interaction between upstream curvature and slope advantage is smoothly  
560 dependent on the relative intensity of the forcings (*Kleinhans et al.*, 2008; *van Dijk et al.*,

561 2014), while this is not the case under super-resonant conditions, for which abrupt transitions  
562 between opposite, highly unbalanced equilibrium states are expected.

563 4. The above results highlight how river bifurcations behave as dynamical systems like many  
564 other eco-morphological processes in rivers and freshwater bodies (e.g. *Scheffer et al.*, 2001),  
565 where the nonlinear interaction among internal and external mechanisms gives rise to a  
566 complex response, characterized by sensitivity to the initial conditions, multistable states  
567 and hysteresis cycles.

## 568 Acknowledgements

569 Marco Redolfi’s work is supported by “Agenzia Provinciale per le Risorse Idriche e l’Energia  
570 (APRIE) - Provincia Autonoma di Trento”. All data are from published works. Matlab codes for  
571 the model solution and for the computation of the resonant aspect ratio are available at [https://](https://bitbucket.org/Marco_Redolfi/freeforced_bifurcations)  
572 [bitbucket.org/Marco\\_Redolfi/freeforced\\_bifurcations](https://bitbucket.org/Marco_Redolfi/freeforced_bifurcations) and at [https://bitbucket.org/](https://bitbucket.org/Marco_Redolfi/bars_res-crit)  
573 [Marco\\_Redolfi/bars\\_res-crit](https://bitbucket.org/Marco_Redolfi/bars_res-crit), respectively. This manuscript has highly benefited from the  
574 comments of Chris Paola and Gerard Salter.

## 575 Appendix A: Fully developed flow in a constant curvature channel

576 Here we provide a detailed derivation of the flow field in a channel of constant curvature, obtained  
577 by following the *Struiksmma et al.* (1985) approach.

578 The model is formulated in a curvilinear system of reference  $\{x, y\}$ , where  $x$  is pointing in the  
579 downstream direction and  $y$  represents the transverse coordinate (see Figure 3). Assuming a fully  
580 developed flow, all dependent variables vary only with  $y$ , and therefore the  $x$ -derivatives vanish; in  
581 such conditions, the continuity equation gives zero transverse fluxes of water and sediment, while  
582 the longitudinal momentum equation reduces to an uniform flow relation for the depth-averaged  
583 longitudinal velocity  $U$ , namely:

$$U = c \sqrt{g S D}, \tag{A1}$$



584 where the longitudinal slope  $S$  depends on  $y$  as:

$$S = S_0 \frac{R}{R + y}, \quad (\text{A2})$$

585 with  $S_0$  indicating the slope of the channel centreline (i.e. at  $y = 0$ ).

586 The longitudinal velocity generates a shear stress  $\tau_x$ , which can be computed as:

$$\tau_x = \rho \frac{U^2}{c^2}, \quad (\text{A3})$$

587 while the secondary flow produces a shear stress in the transverse direction, given by (see *Struiksm*  
588 *et al.*, 1985):

$$\tau_y = -\rho A \frac{DU^2}{c^2} \frac{1}{R}, \quad (\text{A4})$$

589 where  $\rho$  indicates the water density.

590 The transverse stress  $\tau_y$  needs to be compensated by a gradient of the bed elevation. There-  
591 fore, considering the *Ikeda* (1982) formulation for the effect of gravity on the sediment transport  
592 direction, the following relation arises:

$$\frac{r}{\sqrt{\theta}} \frac{d\eta}{dy} = \frac{\tau_y}{\tau_x} = -A \frac{D}{R}. \quad (\text{A5})$$

593 Transverse profiles of bed elevation can be obtained by integrating Equation (A5). To this  
594 aim, we need to specify how the water depth varies along the cross section through the following  
595 geometrical relation:

$$\frac{dD}{dy} = \frac{dH}{dy} - \frac{d\eta}{dy}, \quad (\text{A6})$$

596 where  $H$  indicates the water surface elevation.

597 Under the hypothesis of horizontal free surface, Equation (A6) reduces to  $dD/dy = -d\eta/dy$ ,  
598 so that the differential equation (A5) can be easily solved in terms of  $D$ . More generally, the

599 gradient of free surface elevation can be derived from the equation of transverse momentum:

$$g \frac{dH}{dy} + \frac{\tau_y}{\rho D} = \frac{U^2}{R}, \quad (\text{A7})$$

600 which, when combined with Equations (A5) and (A6), gives an expression of the type:

$$\frac{dD}{dy} = fct(y, D), \quad (\text{A8})$$

601 which can be easily solved by numerical integration.

602 The effect of the channel curvature on the transverse profiles of bed and water surface elevation  
 603 is illustrated in Figure 13. The spiral flow induces higher bed elevation and slightly lower water  
 604 surface elevation at the inner bend. Consequently, water depth, velocity, and water and sedi-  
 605 ment fluxes are higher at the outer bend. The resulting transverse profiles are clearly nonlinear,  
 606 especially when the channel is highly curved.

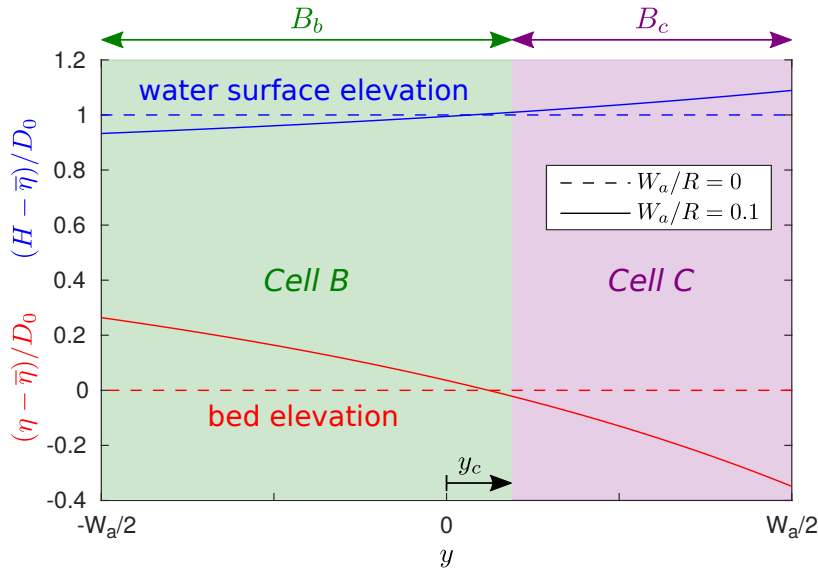


Figure 13: Transverse profiles of (scaled) bed and water surface elevation in the main channel, where  $\bar{\eta}$  is the mean bed elevation. Dashed lines: straight channel; solid lines: curved channel. Parameters are  $\theta_0 = 0.1$ ,  $d_s = 0.02$ ,  $r = 0.5$ . Background colours indicate the position of the two cells of size  $B_b$  and  $B_c$ .

607 Once the transverse profiles are known, the input fluxes for the two-cell model can be com-  
 608 puted by integrating along their respective domain. In the general case of different width of the

609 downstream bifurcates (i.e.  $W_b \neq W_c$ ), the width of the two cells (see Figure 13) can be calculated  
 610 as:

$$B_b = W_a \frac{W_b}{W_b + W_c}, \quad B_c = W_a \frac{W_c}{W_b + W_c}, \quad (\text{A9})$$

611 so that the transverse position of the interface between the two cells reads:

$$y_c = B_b - \frac{W_a}{2} = \frac{W_a}{2} \left( \frac{W_b - W_c}{W_b + W_c} \right), \quad (\text{A10})$$

612 which vanishes when  $W_b = W_c$  as assumed in the paper. Finally, water and sediment fluxes feeding  
 613 the two cells are given by the following relations:

$$Q_b^{IN} = \int_{-W_a/2}^{y_c} UD \, dy, \quad Q_c^{IN} = 1 - Q_b^{IN}, \quad (\text{A11})$$

614

$$Q_{s_b}^{IN} = \sqrt{g\Delta d_{50}^3} \int_{-W_a/2}^{y_c} \Phi \left( \theta, \frac{D}{d_{50}} \right) dy, \quad Q_{s_c}^{IN} = 1 - Q_{s_b}^{IN}. \quad (\text{A12})$$

## 615 **Appendix B: Algebraic expression for $c_D$ , $\Phi_D$ and $\Phi_T$ coefficients**

616 In this section we provide an explicit expression of the coefficients arising from linear stability  
 617 analysis, which are needed to evaluate the critical and the resonant aspect ratio through Equations  
 618 (12) and (14).

619 The  $c_D$  coefficient, which defines the response of the Chézy coefficient to variations of water  
 620 depth, is defined as:

$$c_D := \frac{D_0}{c_0} \frac{\partial c}{\partial D} \Big|_{D_0}. \quad (\text{B1})$$

621 When considering the logarithmic formula of *Engelund and Fredsoe* (1982) (Equation (3)), we  
 622 obtain:

$$c_D = \frac{2.5}{c_0}. \quad (\text{B2})$$

623 where  $c_0$  is the Chézy coefficient evaluated at reference conditions, namely:

$$c_0 = 6 + 2.5 \log \left( \frac{1}{2.5 d_s} \right). \quad (\text{B3})$$

624 Similarly, the coefficients  $\Phi_D$  and  $\Phi_T$ , which specify the sensitivity of the sediment transport  
 625 to variations of water depth and Shields stress, are defined as:

$$\Phi_D := \frac{D_0}{\Phi_0} \frac{\partial \Phi}{\partial D} \Big|_{\theta_0, D_0}, \quad \Phi_T := \frac{\theta_0}{\Phi_0} \frac{\partial \Phi}{\partial \theta} \Big|_{\theta_0, D_0}, \quad (\text{B4})$$

626 and their explicit expression depends on the sediment transport formula used.

627 The *Engelund and Hansen* (1967) transport formula reads:

$$\Phi = 0.05 c^2 \theta^{2.5}, \quad (\text{B5})$$

628 and gives the following coefficients:

$$\Phi_D = 2 c_D, \quad \Phi_T = 2.5. \quad (\text{B6})$$

629 Transport formulae designed for bed load are often expressed in terms of  $\theta$  only, and therefore  
 630  $\Phi_D$  vanishes as the bed load function does not depend explicitly on water depth. For example  
 631 when using the *Meyer-Peter and Muller* (1948) relation

$$\Phi = 8 (\theta - \theta_{cr})^{1.5} \quad (\text{B7})$$

632 the coefficients reads:

$$\Phi_D = 0, \quad \Phi_T = 1.5 \frac{\theta_0}{\theta_0 - \theta_{cr}}. \quad (\text{B8})$$

633 The *Parker* (1990) formula can be expressed as:

$$\Phi = 0.00218 \theta^{1.5} G(\xi), \quad \xi := \frac{\theta}{0.0386}, \quad (\text{B9})$$

634 where  $G(\xi)$  is a piecewise-defined function:

$$G(\xi) = \begin{cases} 5474 (1 - 0.853/\xi)^{4.5} & \xi > 1.59 \\ \exp [14.2(\xi - 1) - 9.28(\xi - 1)^2] & 1 \leq \xi \leq 1.59 \\ \xi^{14.2} & \xi < 1 \end{cases} . \quad (\text{B10})$$

635 In this case we obtain:

$$\Phi_D = 0, \quad \Phi_T = 1.5 + \frac{G_\xi}{0.0386}, \quad G_\xi := \frac{\xi_0}{G_0} \frac{dG}{d\xi}, \quad (\text{B11})$$

636 where  $G_\xi$  can be expressed by deriving Equation (B10), which gives:

$$G_\xi = \begin{cases} \frac{4.5}{\xi_0/0.853 - 1} & \xi_0 > 1.59 \\ -18.56 \xi_0^2 + 32.76 \xi_0 & 1 \leq \xi_0 \leq 1.59 \\ 14.2 & \xi_0 < 1 \end{cases} . \quad (\text{B12})$$

## 637 **References**

- 638 Baar, A. W., J. de Smit, W. S. J. Uijttewaal, and M. G. Kleinhans (2018), Sediment Transport of  
639 Fine Sand to Fine Gravel on Transverse Bed Slopes in Rotating Annular Flume Experiments,  
640 *Water Resources Research*, *54*(1), 19–45, doi:10.1002/2017WR020604.
- 641 Bertoldi, W. (2012), Life of a bifurcation in a gravel-bed braided river, *Earth Surface Processes*  
642 *and Landforms*, *37*(12), 1327–1336, doi:10.1002/esp.3279.
- 643 Bertoldi, W., and M. Tubino (2007), River bifurcations: Experimental observations on equilibrium  
644 configurations, *Water Resources Research*, *43*(10), 1–10, doi:10.1029/2007WR005907.
- 645 Bertoldi, W., L. Zanoni, S. Miori, R. Repetto, and M. Tubino (2009), Interaction between mi-  
646 grating bars and bifurcations in gravel bed rivers, *Water Resources Research*, *45*(6), 1–12,  
647 doi:10.1029/2008WR007086.
- 648 Blondeaux, P., and G. Seminara (1985), A Unified Bar Bend Theory of River Meanders, *Journal*  
649 *of Fluid Mechanics*, *157*, 449–470.
- 650 Bolla Pittaluga, M., R. Repetto, and M. Tubino (2003), Correction to “Channel bifurcation in  
651 braided rivers: Equilibrium configurations and stability”, *Water Resources Research*, *39*(3),  
652 1–13, doi:10.1029/2003WR002754.
- 653 Bolla Pittaluga, M., G. Coco, and M. G. Kleinhans (2015), A unified framework for stability of  
654 channel bifurcations in gravel and sand fluvial systems, *Geophysical Research Letters*, *42*(18),  
655 7521–7536, doi:10.1002/2015GL065175.
- 656 Burge, L. M. (2006), Stability, morphology and surface grain size patterns of channel bifurcation  
657 in gravel-cobble bedded anabranching rivers, *Earth Surface Processes and Landforms*, *31*(10),  
658 1211–1226, doi:10.1002/esp.1325.
- 659 Camporeale, C., P. Perona, A. Porporato, and L. Ridolfi (2007), Hierarchy of models for me-  
660 andering rivers and related morphodynamic processes, *Reviews of Geophysics*, *45*(1), 1–28,  
661 doi:10.1029/2005RG000185.

- 662 Edmonds, D. A. (2012), Stability of backwater-influenced river bifurcations: A study of  
663 the Mississippi-Atchafalaya system, *Geophysical Research Letters*, *39*(8), 1–5, doi:10.1029/  
664 2012GL051125.
- 665 Edmonds, D. A., and R. L. Slingerland (2008), Stability of delta distributary networks and their  
666 bifurcations, *Water Resources Research*, *44*(9), 1–13, doi:10.1029/2008WR006992.
- 667 Englund, F., and J. Fredsoe (1982), Sediment Ripples and Dunes, *Annual Review of Fluid Me-*  
668 *chanics*, *14*, 13–37, doi:10.1146/annurev.fl.14.010182.000305.
- 669 Englund, F., and E. Hansen (1967), *A monograph on sediment transport in alluvial streams*, 65  
670 pp., Tekniks Forlag, Copenhagen, Denmark, doi:10.1007/s13398-014-0173-7.2.
- 671 Federici, B., and C. Paola (2003), Dynamics of channel bifurcations in noncohesive sediments,  
672 *Water Resources Research*, *39*(6), 1162, doi:10.1029/2002WR001434.
- 673 Golubitsky, M., and D. Schaeffer (1979), An analysis of imperfect bifurcation, *Annals of the New*  
674 *York Academy of Sciences*, *316*(1), 127–133, doi:10.1111/j.1749-6632.1979.tb29464.x.
- 675 Grenfell, M., R. Aalto, and A. Nicholas (2012), Chute channel dynamics in large, sand-bed mean-  
676 dering rivers, *Earth Surface Processes and Landforms*, *37*(3), 315–331, doi:10.1002/esp.2257.
- 677 Habersack, H., and H. Piégay (2007), 27 River restoration in the Alps and their surroundings:  
678 past experience and future challenges, *Developments in Earth Surface Processes*, *11*, 703–735.
- 679 Hardy, R. J., S. N. Lane, and D. Yu (2011), Flow structures at an idealized bifurcation: A  
680 numerical experiment, *Earth Surface Processes and Landforms*, *36*(15), 2083–2096, doi:10.1002/  
681 esp.2235.
- 682 Ikeda, S. (1982), Incipient motion of sand particles on side slopes, *Journal of Hydraulic Division*,  
683 *108*(1), 95–114.
- 684 Kleinhans, M. G., B. Jagers, E. Mosselman, and K. Sloff (2006), Effect of upstream meanders on  
685 bifurcation stability and sediment division in 1D, 2D and 3D models, in *River flow 2006 : pro-*

686 *ceedings of the International Conference on Fluvial Hydraulics, Lisbon, Portugal, 6-8 September*  
687 *2006*, pp. 1355–1362.

688 Kleinans, M. G., H. R. A. Jagers, E. Mosselman, and C. J. Sloff (2008), Bifurcation dynamics  
689 and avulsion duration in meandering rivers by one-dimensional and three-dimensional models,  
690 *Water Resources Research*, *44*(8), 1–31, doi:10.1029/2007WR005912.

691 Kleinans, M. G., K. M. Cohen, J. Hoekstra, and J. M. Ijmker (2011), Evolution of a bifurcation  
692 in a meandering river with adjustable channel widths, Rhine delta apex, The Netherlands, *Earth*  
693 *Surface Processes and Landforms*, *36*(15), 2011–2027, doi:10.1002/esp.2222.

694 Kleinans, M. G., T. de Haas, E. Lavooi, and B. Makaske (2012), Evaluating competing hypothe-  
695 ses for the origin and dynamics of river anastomosis, *Earth Surface Processes and Landforms*,  
696 *37*(12), 1337–1351, doi:10.1002/esp.3282.

697 Kleinans, M. G., R. I. Ferguson, S. N. Lane, and R. J. Hardy (2013), Splitting rivers at their  
698 seams: Bifurcations and avulsion, *Earth Surface Processes and Landforms*, *38*(1), 47–61, doi:  
699 10.1002/esp.3268.

700 Lanzoni, S., and M. Tubino (1999), Grain sorting and bar instability, *Journal of Fluid Mechanics*,  
701 *393*, 149–174, doi:10.1017/S0022112099005583.

702 Le, T., A. Crosato, E. Mosselman, and W. Uijttewaai (2018a), On the stability of river bifurcations  
703 created by longitudinal training walls. Numerical investigation, *Advances in Water Resources*,  
704 *113*, 112–125, doi:10.1016/j.advwatres.2018.01.012.

705 Le, T. B., A. Crosato, and W. S. Uijttewaai (2018b), Long-term morphological developments of  
706 river channels separated by a longitudinal training wall, *Advances in Water Resources*, *113*,  
707 73–85, doi:10.1016/j.advwatres.2018.01.007.

708 Lesser, G. R., J. A. Roelvink, J. A. van Kester, and G. S. Stelling (2004), Development and  
709 validation of a three-dimensional morphological model, *Coastal Engineering*, *51*(8-9), 883–915,  
710 doi:10.1016/j.coastaleng.2004.07.014.



- 711 Meyer-Peter, E., and R. Muller (1948), Formulas for bed load transport, *Proceedings of the 2nd*  
712 *congress of the International Association for Hydraulic Research*, 2, 39–64.
- 713 Miori, S., R. Repetto, and M. Tubino (2006), A one-dimensional model of bifurcations in  
714 gravel bed channels with erodible banks, *Water Resources Research*, 42(11), 1–12, doi:  
715 10.1029/2006WR004863.
- 716 Parker, G. (1990), Surface-based bedload transport relation for gravel rivers, *Journal of Hydraulic*  
717 *Research*, 28(4), 417–436, doi:10.1080/00221689009499058.
- 718 Redolfi, M., G. Zolezzi, and M. Tubino (2016), Free instability of channel bifurcations and mor-  
719 phodynamic influence, *Journal of Fluid Mechanics*, 799, 476–504, doi:10.1017/jfm.2016.389.
- 720 Salter, G., C. Paola, and V. R. Voller (2018), Control of Delta Avulsion by Downstream Sed-  
721 iment Sinks, *Journal of Geophysical Research: Earth Surface*, pp. 1060–1067, doi:10.1002/  
722 2017JF004350.
- 723 Scheffer, M., S. Carpenter, J. A. Foley, C. Folke, and B. Walker (2001), Catastrophic shifts in  
724 ecosystems, *Nature*, 413(6856), 591–596, doi:10.1038/35098000.
- 725 Seminara, G., and M. Tubino (1989), Alternate Bars and Meandering : Free , Forced and Mixed  
726 Interactions, in *River Meandering*, vol. 12, edited by S. Ikeda and G. Parker, pp. 267 – 320,  
727 AGU, Washington, D.C.
- 728 Siviglia, A., G. Stecca, D. Vanzo, G. Zolezzi, E. F. Toro, and M. Tubino (2013), Numerical  
729 modelling of two-dimensional morphodynamics with applications to river bars and bifurcations,  
730 *Advances in Water Resources*, 52, 243–260, doi:10.1016/j.advwatres.2012.11.010.
- 731 Slingerland, R., and N. D. Smith (2004), River Avulsions and Their Deposits, *Annu. Rev. Earth*  
732 *Planet. Sci.*, 32(1), 257–285, doi:10.1146/annurev.earth.32.101802.120201.
- 733 Sloff, K., and E. Mosselman (2012), Bifurcation modelling in a meandering gravel-sand bed river,  
734 *Earth Surface Processes and Landforms*, 37(14), 1556–1566, doi:10.1002/esp.3305.

735 Struiksmā, N., K. W. Olesen, C. Flokstra, and H. J. De Vriend (1985), Bed deformation in curved  
736 alluvial channels, *Journal of Hydraulic Research*, *23*(1), 57–79, doi:10.1080/00221688509499377.

737 Szupiany, R. N., M. L. Amsler, J. Hernandez, D. R. Parsons, J. L. Best, E. Fornari, and A. Trento  
738 (2012), Flow fields, bed shear stresses, and suspended bed sediment dynamics in bifurcations of  
739 a large river, *Water Resources Research*, *48*(11), 1–20, doi:10.1029/2011WR011677.

740 Tubino, M., and G. Seminara (1990), Free–forced interactions in developing meanders and suppres-  
741 sion of free bars, *Journal of Fluid Mechanics*, *214*, 131–159, doi:10.1017/S0022112090000088.

742 Van der Mark, C. F., and E. Mosselman (2013), Effects of helical flow in one-dimensional modelling  
743 of sediment distribution at river bifurcations, *Earth Surface Processes and Landforms*, *38*(5),  
744 502–511, doi:10.1002/esp.3335.

745 van Dijk, W. M., F. Schuurman, W. I. V. D. Lageweg, and M. G. Kleinhans (2014), Bifurcation  
746 instability and chute cutoff development in meandering gravel-bed rivers, *Geomorphology*, *213*,  
747 277–291, doi:10.1016/j.geomorph.2014.01.018.

748 Wang, Z., M. De Vries, R. Fokkink, and A. Langerak (1995), Stability of river bifurca-  
749 tions in 1D morphodynamic models, *Journal of Hydraulic Research*, *33*(6), 739–750, doi:  
750 10.1080/00221689509498549.

751 Wiggins, S. (2003), *Introduction to Applied Nonlinear Dynamical Systems and Chaos, Texts in*  
752 *Applied Mathematics*, vol. 2, Springer-Verlag, New York, doi:10.1007/b97481.

753 Zhang, W., H. Feng, A. J. F. Hoitink, Y. Zhu, F. Gong, and J. Zheng (2017), Tidal impacts on the  
754 subtidal flow division at the main bifurcation in the Yangtze River Delta, *Estuarine, Coastal*  
755 *and Shelf Science*, *196*, 301–314, doi:10.1016/j.ecss.2017.07.008.

756 Zolezzi, G., and G. Seminara (2001), Downstream and upstream influence in river meandering.  
757 Part 1. General theory and application to overdeepening, *Journal of Fluid Mechanics*, *438*,  
758 213–230, doi:10.1017/S002211200100427X.

759 Zolezzi, G., M. Guala, D. Termini, and G. Seminara (2005), Experimental observations of upstream  
760 overdeepening, *Journal of Fluid Mechanics*, 531, 191–219, doi:10.1017/S0022112005003927.

761 Zolezzi, G., W. Bertoldi, and M. Tubino (2006), Morphological analysis and prediction of river  
762 bifurcations, in *Braided Rivers: Process, Deposits, Ecology and Management*, vol. 36, edited by  
763 G. H. Best, J. L. Bristow, and C. S. Petts, pp. 233–256, Blackwell, doi:10.1002/9781444304374.  
764 ch11.

765 Zolezzi, G., R. Luchi, and M. Tubino (2009), Morphodynamic regime of gravel bed, single-  
766 thread meandering rivers, *Journal of Geophysical Research: Earth Surface*, 114(1), doi:  
767 10.1029/2007JF000968.